

The significance of dynamical architecture for adaptive responses to mechanical loads during rhythmic behavior

Kendrick M. Shaw · David N. Lyttle · Jeffrey P. Gill ·
Miranda J. Cullins · Jeffrey M. McManus · Hui Lu ·
Peter J. Thomas · Hillel J. Chiel

Received: 6 October 2013 / Revised: 25 June 2014 / Accepted: 22 July 2014
© Springer Science+Business Media New York 2014

Abstract Many behaviors require reliably generating sequences of motor activity while adapting the activity to

Action Editor: J. Rinzel

K. M. Shaw (✉)
Department of Biology and Medical Scientist Training Program,
Case Western Reserve University, 10900 Euclid Ave., Cleveland
OH 44106, USA
e-mail: kms15@case.edu

D. N. Lyttle
Departments of Mathematics and Biology, Case Western Reserve
University, 10900 Euclid Ave., Cleveland OH 44106, USA
e-mail: david.lyttle@case.edu

J. P. Gill · M. J. Cullins · J. M. McManus · H. Lu
Department of Biology, Case Western Reserve University, 10900
Euclid Ave., Cleveland OH 44106, USA

J. P. Gill
e-mail: jpg18@case.edu,

M. J. Cullins
e-mail: mjc35@case.edu,

J. M. McManus
e-mail: jmm45@case.edu,

H. Lu
e-mail: hxl75@case.edu,

P. J. Thomas
Mathematics, Applied Mathematics and Statistics, Case Western
Reserve University, 10900 Euclid Ave., Cleveland OH 44106,
USA
e-mail: pjthomas@case.edu

H. J. Chiel
Departments of Biology, Neurosciences and Biomedical
Engineering, Case Western Reserve University, 10900 Euclid
Ave., Cleveland OH 44106, USA
e-mail: hjc@case.edu

incoming sensory information. This process has often been conceptually explained as either fully dependent on sensory input (a chain reflex) or fully independent of sensory input (an idealized central pattern generator, or CPG), although the consensus of the field is that most neural pattern generators lie somewhere between these two extremes. Many mathematical models of neural pattern generators use limit cycles to generate the sequence of behaviors, but other models, such as a heteroclinic channel (an attracting chain of saddle points), have been suggested. To explore the range of intermediate behaviors between CPGs and chain reflexes, in this paper we describe a nominal model of swallowing in *Aplysia californica*. Depending upon the value of a single parameter, the model can transition from a generic limit cycle regime to a heteroclinic regime (where the trajectory slows as it passes near saddle points). We then study the behavior of the system in these two regimes and compare the behavior of the models with behavior recorded in the animal *in vivo* and *in vitro*. We show that while both pattern generators can generate similar behavior, the stable heteroclinic channel can better respond to changes in sensory input induced by load, and that the response matches the changes seen when a load is added *in vivo*. We then show that the underlying stable heteroclinic channel architecture exhibits dramatic slowing of activity when sensory and endogenous input is reduced, and show that similar slowing with removal of proprioception is seen *in vitro*. Finally, we show that the distributions of burst lengths seen *in vivo* are better matched by the distribution expected from a system operating in the heteroclinic regime than that expected from a generic limit cycle. These observations suggest that generic limit cycle models may fail to capture key aspects of *Aplysia* feeding behavior, and that alternative architectures such as heteroclinic channels may provide better descriptions.

Keywords *Aplysia* · Heteroclinic channel · Central pattern generator · Chain reflex · Limit cycle

1 Introduction

Motor behaviors, such as cat running, crayfish swimming, and dog lapping all require the nervous system to reliably generate a sequence of motor outputs. To be efficient, however, a fixed sequence of activity is not enough: a cat that fails to step over an obstacle may lose its footing and fall (Forssberg et al. 1975; Forssberg 1979) and a crayfish that wanders into a current of cold water must control muscles that may suddenly have become stronger but relax more slowly (Harri and Florey 1977). Sensory feedback plays a key role in allowing an animal to adapt its behavioral pattern to the circumstances in which it finds itself. The way that this sensory information is integrated into pattern generation to produce adaptive behavior, however, can be difficult to ascertain.

Historically, two competing theories have been proposed for how the nervous system can generate sequences of motor activity (Marder and Bucher 2001). At one extreme, Loeb (1899) proposed that sensory input is required for the transitions between behaviors, so that the sequence of behavior is formed of a chain of reflexes each leading to the next. He thus proposed calling this form of pattern generation a “kettenreflex,” or “chain reflex.” For example, during walking, this theory would predict that extension of the leg continues until sensory input indicates that the foot has struck the ground, and in the absence of this sensory input, the pattern would not progress. This theory was later elaborated by Sherrington, who noted that bouts of walking-like movements could be evoked in the hind limbs of a dog after spinal transection by dropping the limb, and these motor patterns would stop abruptly when the limb was passively mechanically arrested (Sherrington 1910).

Even the strongest proponents of chain reflex theory saw it as an incomplete explanation of what was observed in the biology, however. Sherrington, noting that spinal stimulation could produce step-like movements even in a deafferented limb, concluded “These difficulties suggest that generation of a secondary local stimulus and its interference with the operation of the primary remote stimulus, although regulative of the rhythm (cf. vagus and respiratory rhythm) is of itself not the sole rhythm-producing factor in the reflex.” By the time Wilson showed that the nervous system in the locust could generate strong structured motor patterns in the absence of sensory input (Wilson 1961), investigators had come to assume that sequences of motor activity were primarily generated by a central pattern generator. The central pattern generator theory suggests that the nervous system can, on its own, produce

appropriate patterns of motor activity even in the absence of sensory input. Within the context of this theory, sensory input merely serves to modulate the underlying neural pattern.

It should be noted, however, that patterns generated by the isolated nervous system often are very distorted compared to those seen *in vivo*. In particular, components of the motor pattern are often significantly longer than those observed in the intact animal. This observation has led many investigators to question the descriptive power of central pattern generator theory. In the words of Robertson and Pearson, “Although now abundantly clear that a central rhythm generator can produce powerful oscillations in the activity of flight motor neurons and interneurons [in locusts], it is equally clear that the properties of this central oscillator cannot fully account for the normal flight pattern” (Selverston 1985).

There is some evidence that slowing of isolated neural patterns may be due to the absence of sensory feedback and endogenous input. In Pearson et al. (1983), cycle-by-cycle stimulation of the appropriate sensory afferents was able to restore wing-beat frequency in fictive flight in the locust. Restoration of the normal pattern by sensory input suggests that biological pattern generators may occupy a middle ground between pure central pattern generators and chain reflexes. In some cases, endogenous neural input may control where a system lies on this continuum. As Bässler (1986) noted when considering a relaxation-oscillator like model of a central pattern generator “Hence, one and the same system can behave either like a CPG or like a chain reflex, depending only on the amount of endogenous input.” These investigators thus warned about the dangers of inferring the mechanism used by a pattern generator *in vivo* based only on the behavior of a pattern generator *in vitro*.

Despite these hesitations, the empirical data supporting the central pattern generator hypothesis led to a focus on providing a mathematical formulation for this theory using the qualitative analysis of dynamical systems. The behavior of an ideal central pattern generator naturally corresponds to a system of nonlinear ordinary differential equations whose solutions contain a stable limit cycle (an attracting isolated periodic orbit). As a result, this structure has played a central role in the mathematical description of central pattern generators (Ijspeert 2008).

In contrast, there have been fewer attempts to model chain reflexes with systems of differential equations. Instead, much of the work modeling these types of sensory-dependent systems uses different tools, such as finite state machines (Lewinger et al. 2006). While these models can capture individual phases of the behavior well, they generally do not describe the transitions between the phases, which may be important in understanding some forms of behavior. In contrast, one could view the state of a chain

reflex system in terms of a series of stable fixed points. In each phase of the motion, the trajectory would be captured by one of the fixed points until the appropriate (external) sensory input pushed the system out of the neighborhood attracted to that fixed point and into the basin of attraction of the next.

Between these two extremes of models of central pattern generators and chain reflexes, one may consider systems in which the progress of a periodic orbit is slowed, but not stopped, by passage near one or more fixed points. This behavior arises naturally in a structure known as a “stable heteroclinic channel” (Rabinovich et al. 2008), where multiple saddle points (fixed points that attract in some directions while repelling in others) are connected in a cycle, so that the unstable manifold of each saddle point brings the system near the stable manifold of the next fixed point. This structure has been used to describe motor behavior such a predatory swimming behavior in *Clione* (Levi et al. 2004; Varona et al. 2004). To our knowledge, however, these models of pattern generation have not been directly compared to those built with a more “pure” limit cycle that does not pass near fixed points.

A potential advantage of a dynamical system that allows trajectories to move close to equilibrium points is that it may spend longer or shorter times in that vicinity, rather than proceeding through the cycle with a relatively constant velocity. In turn, this could allow an animal greater flexibility in responding to unexpected changes in the environment, such as increases or decreases in mechanical load as it attempts to manipulate an object. Other studies have investigated dynamical architectures in which oscillatory pattern generators can selectively slow their dynamics in response to sensory input (Zhang and Lewis 2013; Büschges and Gruhn 2007; Daun-Gruhn and Büschges 2011; Nadim et al. 2011; Rowat and Selverston 1993), which we discuss in Section 6.2.2.

To examine these alternative dynamical architectures, we have created a neuromechanical model based on the feeding apparatus of the marine mollusk *Aplysia californica*. We examine the behavior of the model in two parameter regimes. In the first parameter regime, the neural dynamics are largely insensitive to sensory feedback, and produce output similar to an idealized central pattern generator. In this regime, the presence of equilibrium points has only a small effect, and the neural dynamics behave like a limit cycle. In the second parameter regime, proprioceptive feedback can overcome the intrinsic neural dynamics and selectively slow progression through different points of the cycle, thereby producing behavior closer to that of a chain reflex. In this regime, the stable heteroclinic channel structure becomes important, since the presence of the equilibrium points is the key dynamical feature allowing the sensory feedback to selectively slow the dynamics. We then compare the

behavior of the two models to the observed behavior of the animal, and show that several of the features of the animal’s behavior are better described by the model in the more “chain-reflex like” parameter regime. At the end of the paper, we reflect on possible general principles suggested by this work.

2 Mathematical framework

In this section we describe a general mathematical framework we will use for modeling the behavior of motor pattern generators. We model a central pattern generator receiving sensory input from the body as a system of differential equations specifying the evolution of a vector of n neural state variables, $\mathbf{a} \in \mathbb{R}^n$, and a vector of m state variables, $\mathbf{x} \in \mathbb{R}^m$, representing the mechanics and periphery (e.g. muscle activation). We assume that an applied load interacts only with the mechanical state variables, so that the differential equations can be naturally written in the following form:

$$\frac{d\mathbf{a}}{dt} = f(\mathbf{a}, \boldsymbol{\mu}) + \epsilon g(\mathbf{a}, \mathbf{x}), \quad (1)$$

$$\frac{d\mathbf{x}}{dt} = h(\mathbf{a}, \mathbf{x}) + \zeta l(\mathbf{x}). \quad (2)$$

Here $\boldsymbol{\mu}$ is a vector of parameters which can encode states such as arousal of the animal, $f(\mathbf{a}, \boldsymbol{\mu})$ represents the intrinsic dynamics of a motor pattern generator, $h(\mathbf{a}, \mathbf{x})$ represents the dynamics of the periphery with the given central input, $g(\mathbf{a}, \mathbf{x})$ represents the effects of sensory feedback from the periphery, $l(\mathbf{x})$ represents the effects of an external load or perturbation, and $\epsilon, \zeta \in \mathbb{R}^+$ are scaling constants, not necessarily small. We further assume that all of these functions have bounded ranges over the domain of interest.

2.1 Limit cycles

We first consider the case of an idealized central pattern generator, where a part of the nervous system can produce sequences of motor activity that closely resemble those seen *in vivo*, even when it is not attached to the periphery. Thus we assume that, for some range of the parameter $\boldsymbol{\mu}$, the dynamics of the isolated neural circuit, $d\mathbf{a}/dt = f(\mathbf{a}, \boldsymbol{\mu})$, contain an attracting limit cycle $\chi(t)$ which represents the observed motor pattern.

2.2 Chain reflex models

We next consider the chain reflex. In this case, the dynamics of the isolated nervous system, $d\mathbf{a}/dt = f(\mathbf{a}, \boldsymbol{\mu})$, will contain a set of stable nodes, A , where each node

represents a “stage” of the chain reflex, that can be destabilized by sensory input. Note that in this case, unlike the central pattern generator, ϵ may need to be large to destabilize a node. The combined dynamics of the nervous system and the periphery, however, would still be expected to contain a stable limit cycle $\xi(t)$ rather than a series of fixed points. Similar dynamics have been seen in models of other biological oscillators; for example in Novak et al. (1998) the authors created a model of the cell cycle where fixed points in the biochemical dynamics (analogous to the isolated neural dynamics) can be destabilized by changes in cell size (analogous to the periphery) so that the coupled system contains a limit cycle.

2.3 Stable heteroclinic channels

We now consider a system that is intermediate between the two extremes of an idealized central pattern generator and a chain reflex. We can construct such a system from a set of n -dimensional hyperbolic saddle points, each with a one-dimensional unstable manifold and an $n - 1$ dimensional stable manifold, arranged in a cycle such that the unstable manifold of one saddle point intersects the stable manifold of the next, forming a heteroclinic orbit. We refer to these saddle points and their connecting heteroclinic orbits as a *heteroclinic cycle* (Guckenheimer and Holmes 1988).

Under appropriate conditions, this heteroclinic cycle attracts nearby orbits (and thus can be called a stable heteroclinic cycle). In particular, if we define the (positive) ratio of the least negative stable eigenvalue $\lambda_{i,s}$ and the unstable eigenvalue $\lambda_{i,u}$ of the i th saddle as the saddle index $\nu_i = -\lambda_{i,s}/\lambda_{i,u}$ (Shilnikov et al. 2002), then the heteroclinic cycle will attract nearby orbits if $\prod_i \nu_i > 1$ (Afraimovich et al. 2004a). This type of dynamics can arise naturally from neural models involving symmetric, mutually inhibitory pools of neurons; for example see (Nowotny and Rabinovich (2007), and Komarov et al. (2013, 2009). Slow switching along heteroclinic loops can also occur in systems of coupled phase oscillators (Kori and Kuramoto 2001). Conditions for the occurrence of stable heteroclinic channels have been studied in Komarov et al. (2010) and Ashwin et al. (2011).

An unperturbed trajectory on the heteroclinic cycle will, like the chain reflex model in Section 2.2, asymptotically approach a fixed point. Unlike the chain reflex model, however, any perturbation transverse to the stable direction will push the trajectory out of the stable manifold, allowing the trajectory to leave the neighborhood of the fixed point (and potentially travel to the neighborhood of the next fixed point). Arbitrarily small amounts of noise can thus ensure that the system will almost certainly not

remain stuck at a given fixed point (Stone and Holmes 1990; Armbruster et al. 2003; Gog et al. 1999). In contrast to the stability of states seen in the chain reflex model, the heteroclinic cycle exhibits metastability (Afraimovich et al. 2011), where the trajectory spends long but finite periods of time near each fixed point (Bakhtin 2011). Thus, like the chain reflex, the system can spend short or long periods of time in one particular state depending on sensory input, but, like the limit cycle, the system will eventually transition to the next state even in the absence of sensory input.

While stable heteroclinic cycles are structurally unstable (i.e. a small change in the vector field will generally break the cycle), small perturbations can result in the creation of a stable limit cycle that passes very close to the saddles. For example, in the planar case, any sufficiently small perturbation that pushes the unstable manifold of the saddles towards the inside of the unperturbed stable heteroclinic cycle will result in a stable limit cycle (Reyn 1980). Similar conditions can be found for higher dimensional stable heteroclinic cycles (Afraimovich et al. 2004a). These families of limit cycles that pass close to the original saddles, known as stable heteroclinic channels (SHCs) (Rabinovich et al. 2008), are structurally stable, and exhibit many of the same properties of sensitivity and metastability as the original stable heteroclinic cycles. As we will see, this extreme sensitivity can be advantageous for generating adaptive behaviors.

In the next section we provide an example of model dynamics $f(\mathbf{a}, \mu)$, parameterized by a scalar parameter μ , that exhibits a limit cycle for $\mu > 0$ and a bifurcation to a heteroclinic cycle at $\mu = 0$. We then demonstrate that the full system (\mathbf{a}, \mathbf{x}) displays an abrupt transition between “limit cycle” and “heteroclinic” dynamics depending on the balance between sensory feedback (ϵ) and intrinsic excitability (μ).

3 Model description

3.1 Neural model

We wish to explore the effects of different types of neural dynamics on the behavior of the animal. Although detailed, multi-cellular and multi-conductance models of neurons and circuits underlying feeding pattern generation in *Aplysia* have been described (Baxter and Byrne 2006; Cataldo et al. 2006; Susswein et al. 2002), the complexity of these models makes it difficult to use them for mathematical analysis. As a consequence, we choose to represent neural pools (which contain neurons that are electrically coupled to one another or have mutual synaptic excitation) using nominal firing-rate models.

As discussed in Section 2, we define the neural dynamics as a combination of an intrinsic component, $f(\mathbf{a}, \mu)$, that does not depend on the periphery, and a sensory (coupling) component, $g(\mathbf{x})$, which does depend on the periphery. For mathematical tractability, we assume that the intrinsic and sensory drive combine linearly, thus giving the evolution equation of the neural activity

$$\frac{d\mathbf{a}}{dt} = f(\mathbf{a}, \mu) + \epsilon g(x_r), \tag{3}$$

where \mathbf{a} is a vector of the activity of each of the N neural pools, ϵ is a parameter scaling the strength of sensory input, x_r is a biomechanical state variable which we will define in more detail in Section 3.2, and μ is a scalar parameter that can shape the intrinsic dynamics.

Specifically, we will consider the following modified Lotka–Volterra model which captures the dynamics of N neural pools:

$$f_i(\mathbf{a}, \mu) = \frac{1}{\tau_a} \left(\left(1 - \sum_j \rho_{ij} a_j \right) a_i + \mu \right), \tag{4}$$

for $0 \leq i < N$. Here μ is a scalar parameter representing intrinsic excitation, τ_a is a time constant, and ρ is the coupling matrix

$$\rho_{ij} = \begin{cases} 1 & i = j \\ \gamma & i = j - 1 \pmod{N} \\ 0 & \text{otherwise,} \end{cases} \tag{5}$$

where γ is a coupling constant representing inhibition between neural pools. In *Aplysia*, the neural pools responsible for motor pattern generation are largely connected via inhibition (Jing et al. 2004). As a first approximation, we assume that the units are identical. Making the inhibitory coupling weaker in one direction than the other is a natural way of encouraging the activation sequence to proceed in a particular direction around the cycle of neural pools.

When $N > 2$ and $\gamma > 2$ this system contains a stable heteroclinic cycle when $\mu = 0$ (Afraimovich et al. 2004a). In contrast, as shown in Fig. 1, it contains a stable limit cycle for small positive values of μ , with the distance between the limit cycle and saddles increasing with increasing values of μ . With the goal of parsimony, we use $N = 3$ and thus (4) can be expanded to

$$f_0(\mathbf{a}, \mu) = \frac{1}{\tau_a} (a_0(1 - a_0 - \gamma a_1) + \mu), \tag{6}$$

$$f_1(\mathbf{a}, \mu) = \frac{1}{\tau_a} (a_1(1 - a_1 - \gamma a_2) + \mu), \tag{7}$$

$$f_2(\mathbf{a}, \mu) = \frac{1}{\tau_a} (a_2(1 - a_2 - \gamma a_0) + \mu). \tag{8}$$

We explain the correspondence of these three neural pools to specific neural pools in *Aplysia* in the next section.

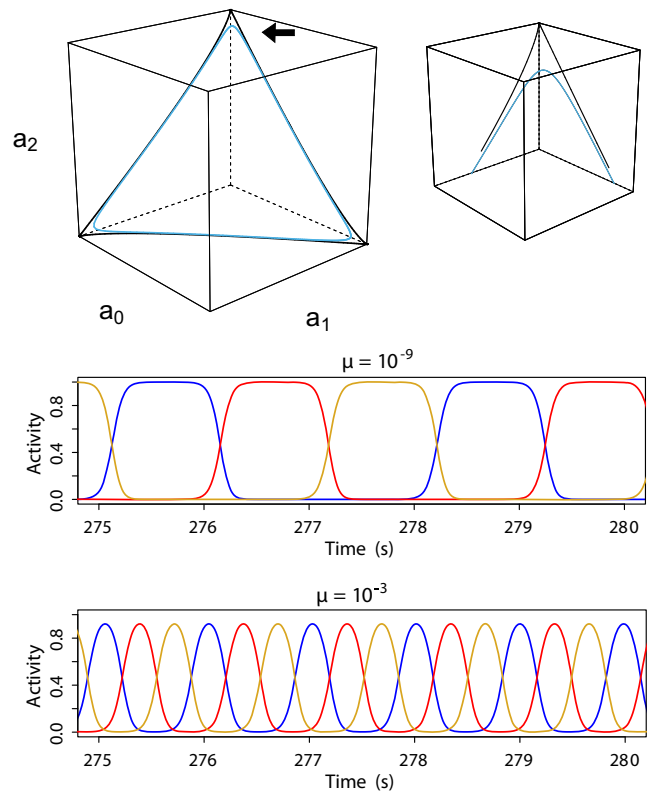


Fig. 1 The endogenous neural excitation parameter μ determines whether the model behaves more like a stable heteroclinic cycle or a limit cycle. *Top left* When $\mu = 0$, in the absence of sensory input ($\epsilon = 0$), the intrinsic neural dynamics contain a stable heteroclinic cycle connecting saddles at $(1, 0, 0)$, $(0, 1, 0)$, and $(0, 0, 1)$. When μ is a small positive number and $\epsilon = 0$, the heteroclinic cycle is broken and a stable limit cycle arises. For very small μ (10^{-9}), the trajectory passes very close to the fixed points (*black line*). For larger values of μ (10^{-3}) the trajectory (shown in *light blue*) does not pass near the fixed points. *Top right* Magnified view of the isolated trajectories of the system near one of the fixed points, (indicated by the arrow in the *top left panel*). The small μ system clearly passes much closer to the fixed points. *Middle* Sample trajectories of the three neural state variables when μ is small (10^{-9}), and no sensory feedback is present. Because in this case the trajectory passes near the fixed points, the dynamics exhibit long dwell times near each fixed point, separated by rapid transitions. Note the relatively long cycle period. *Bottom* Sample trajectories of the neural state variables when μ is larger (10^{-3}). Here the oscillation period is faster, and the variables change less sharply. For these larger values of μ , the effect of the equilibrium points is less evident, and the system behaves like a typical limit cycle

To understand the effects of proprioceptive input (the term $\epsilon g(\mathbf{a}, \mathbf{x})$ in Eq. (1); see Section 3.3), it is important to understand how adding a constant endogenous excitatory drive $\mu > 0$ to each equation changes the geometry of the differential Eqs. (6)–(8). Let Π_0 , Π_1 and Π_2 denote the planes

$$\Pi_0 = \{(0, \alpha, \beta) | (\alpha, \beta) \in \mathbb{R}^2\} \tag{9}$$

$$\Pi_1 = \{(\beta, 0, \alpha) | (\alpha, \beta) \in \mathbb{R}^2\} \tag{10}$$

$$\Pi_2 = \{(\alpha, \beta, 0) | (\alpha, \beta) \in \mathbb{R}^2\}. \tag{11}$$

When $\mu = 0$ each of these planes is a flow-invariant subset of \mathbb{R}^3 for Eqs. (6)–(8). Taking Π_2 as an example, if we begin at point $\mathbf{a} = (\alpha, \beta, 0)$ then $\dot{a}_0 = \alpha(1 - \alpha - \gamma\beta)/\tau_a$, $\dot{a}_1 = \beta(1 - \beta)/\tau_a$, and $\dot{a}_2 = 0$. Flow invariance means that if initial conditions are chosen in plane Π_i , the subsequent trajectory remains in Π_i for all time. Moreover, the heteroclinic trajectories beginning and ending at the saddle fixed points at $(1, 0, 0)$, $(0, 1, 0)$ and $(0, 0, 1)$ lie in the union of these three planes. It is these trajectories to which initial conditions in the interior of the unit cube are attracted, leading to progressive slowing of the orbits.

In contrast, when $\mu > 0$, the Π_i are no longer flow-invariant. Instead, initial conditions on plane Π_i have a velocity component $\dot{a}_i > 0$ moving the trajectory to the interior of the unit cube. By steering trajectories inward in the vicinity of the saddle points, positive μ prevents the unbounded growth of the return time and leads to creation of a finite period attracting limit cycle. As we will see in Section 5.1, inhibitory input from proprioceptive feedback can contribute with sign opposite that of μ , partially undoing this steering effect.

Note that, in the absence of proprioceptive feedback, the neural state variables a_i will remain confined to the domain $(0,1)$. However, with the addition of either proprioceptive feedback (the term $g(x_r)$ in Eq. (3)) or noise, the neural state variables can be pushed out of this domain. Therefore, we impose strict, rectifying boundary conditions on these variables that prevent them from leaving this domain. For neural state variables that have reached the boundary at 0, any inhibitory input is ignored, while for variables that have reached the upper boundary at 1, any further excitatory input is similarly ignored. Biologically, this can be interpreted as assuming that inhibitory input to an inactive neural pool has no effect, whereas excitatory input to a maximally active neural pool similarly has no effect. The $g(x_r)$ term, which describes the proprioceptive feedback from the feeding apparatus, will be described in Section 3.3.

3.2 Model of the periphery and load

We next couple the neural dynamics to a nominal mechanical model of swallowing in *Aplysia*. In the general framework described in Eqs. (1) and (2), the biomechanics with no applied load corresponds to $h(\mathbf{a}, \mathbf{x})$ in (2), and the perturbations applied by the seaweed force correspond to $l(\mathbf{x})$.

During ingestive behaviors in *Aplysia*, a grasper, known as the radula-odontophore, is protracted through the jaws by a muscle referred to as I2. The grasper closes on food, is retracted by a muscle called I3, and then opens again, completing the cycle (see Fig. 2). The timing of closing is often not precisely aligned with the switch from protraction to retraction. Instead, closing usually occurs before the end of protraction, although the amount of overlap varies

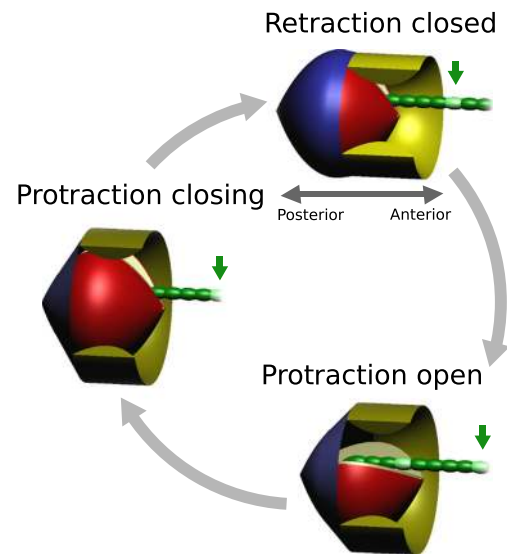


Fig. 2 The model divides swallowing into three phases. First, the grasper protracts while open (*lower right*). Near the end of protraction, the grasper begins closing (*left*) and protracts a small distance while closed. In the last phase, the grasper retracts while closed (*upper right*). The ingestive cycle then repeats. The protraction muscle (I2) is shown in blue, the grasper (the radula-odontophore) is shown in red, and the ring-like retraction muscle (I3) is shown in yellow, with a section cut away to show the grasper. The *green strand* is seaweed, with the *arrows* showing how the seaweed moves within a single cycle

by behavior, from very little overlap in swallows to a significant overlap in egestive behaviors. A general model for biting and swallowing could thus contain four components: protraction while open, protraction while closed, retraction while closed, and retraction while open. For simplicity, we reduce these to three components, each of which corresponds to one of the three neural pools in the neural model: protraction open, protraction closing, and retraction closed, as shown in Fig. 1. The protraction open neural pool (a_0) corresponds to the electrically coupled group of neurons B31, B32, B61, B62, and B63, which activate the I2 muscle and are all active during protraction ((Hurwitz et al. 1996, 1997; Susswein et al. 2002). The protraction closing neuron pool (a_1) corresponds to these same I2 neurons with the addition of the B8 motor neurons, which activate the I4 muscle used in closing (Morton and Chiel 1993). The retraction closed pool (a_2) contains B8 with the addition of the I3 motor neurons B3, B6, and B9 and the interneuron B64 which are simultaneously active during retraction (Church and Lloyd 1994). Thus the I2 muscle will be driven by both protraction-open (a_0) and protraction-closing (a_1) neural pools, whereas the I3 muscle is driven by a single neural pool (a_2).

The I2 and I3 muscles are known to respond slowly to neural inputs (Yu et al. 1999); we thus model their activation as a low-pass filter of the neural inputs using the time constants from the model of the I2 muscle described by

Yu et al. (1999). Using u_i for the activation of the i th muscle and τ_m for the time constant of the filter, we use

$$\frac{du_0}{dt} = \frac{1}{\tau_m}((a_0 + a_1)u_{\max} - u_0), \tag{12}$$

$$\frac{du_1}{dt} = \frac{1}{\tau_m}(a_2u_{\max} - u_1). \tag{13}$$

Note that the muscle activation variables u_i are components of the vector \mathbf{x} of biomechanical variables described in Eq. (2).

In general, the force a muscle can exert will vary with the length to which it is extended (Zajac 1989; Fox and Lloyd 1997). The length-tension relationship is typically explained by the sliding filament theory as follows: for some maximal length, the actin and myosin fibers will not overlap and the muscle will be limited to passive forces, but below that length, the force will first rise with the increasing overlap of the actin and myosin fibers, reach a maximum, and then decline as the overlapping fibers start to exert steric effects (Gordon et al. 1966). More recently, changes in lattice spacing between the fibers have also been shown to have a role in the force-length dependence (Williams et al. 2013). We model this length-tension curve using the following simple cubic polynomial:

$$\phi(x) = -\kappa x(x - 1)(x + 1), \tag{14}$$

where κ is a scaling constant. This equation crosses through zero force at zero length and again reaches zero at the nominal maximal length of 1. We let $\kappa = 3\sqrt{3}/2$ to normalize the maximum force between these two points to 1 (which occurs at a length of $1/\sqrt{3}$).

Although mechanical advantage plays an important role in swallowing (Sutton et al. 2004b; Novakovic et al. 2006), when combined with the length-tension curve, the resulting force resembles a shifted and rescaled version of the original length-tension curve over the range of motion used in swallowing. We thus choose position and scaling constants for the length-tension curve to approximate the resultant force curve in the biomechanics, rather than the length-tension curve of the isolated muscle.

We assume the tension on each muscle is linearly proportional to its activation, and sum all of the muscle forces giving

$$F_{\text{muscle}} = k_0\phi\left(\frac{x_r - c_0}{w_0}\right)u_0 + k_1\phi\left(\frac{x_r - c_1}{w_1}\right)u_1. \tag{15}$$

Here $x_r \in [0, 1]$ is the position of the grasper, k_i is a parameter representing the strength and direction of each muscle, c_i the position of the grasper where the i th muscle is at its minimum effective length, and w_i the difference between the maximum and minimum effective lengths for the i th muscle. The sign of k_i determines the direction of force of the muscle; when k_i is negative (as it is for I2) the muscle will pull towards its position of shortest length, and when it is

positive (as it is for I3) it will push away from this position (in the case of I3, squeezing the grasper out of the ring of the jaws).

We model closing and opening of the grasper (and thus holding and releasing the seaweed) as a simple binary function, where the grasper is closed when certain neural pools are active and open otherwise. Specifically, the grasper is considered to be closed when $a_1 + a_2 \geq 0.5$, and open when $a_1 + a_2 < 0.5$ (see Figure 3). This threshold can be viewed as a plane dividing phase space into two regions with different mechanics (holding the seaweed and not holding the seaweed). The resulting dynamics are piecewise continuous; a similar situation arises at the stance/swing transition in walking (Spardy et al. 2011a, b).

In our experience, the teeth on the radular surface of the grasper tend to hold the seaweed very firmly, and the animal tends to let go before the seaweed slips from its grasp. Thus the seaweed and the grasper are considered to be “locked together” when the grasper is closed and we do not attempt to model slip. The seaweed is assumed to be pulling back with a constant force F_{sw} , which is included in the net force on the grasper when the grasper is closed (see below).

We have observed that when seaweed is abruptly pulled, animals respond with rapid movements of the grasper without oscillations. This suggests that the system is at least critically damped under these conditions, if not over damped. Furthermore, since the mass of the buccal mass is very small (a few grams), and the accelerations during movement are

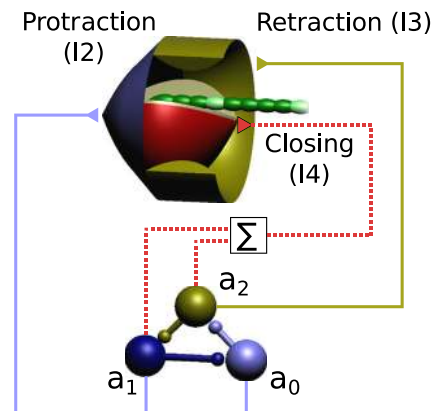


Fig. 3 Schematic of the neuromechanical model of the feeding apparatus in *Aplysia*. The three neural pools (a_0 , a_1 , and a_2) control three phases of swallowing shown in Fig. 2: protraction open, protraction closing, and retraction closed. The solid lines and triangles indicate excitatory synaptic coupling with a neuromuscular transform represented by a low pass filter. The dashed line and summation symbol represent a simple summation and thresholding that control closing in the model. The a_0 neural pool represents the B31, B32, B61, B62, and B63 neurons, the a_1 neural pool represents these same neurons with the addition of B8 (which experiences slow excitation from B34), and the a_2 neural pool represents B64, B3, B6, B9, and B8 (which is excited by B64) activity

typically small (based on MRI measurements, they may be close to zero during most of the motion Neustadter 2002, 2007), we choose to use equations of motion that assume a viscous limit. Additionally, it has been observed that the anterior portion of the I3 muscle can act to hold seaweed in place while the grasper is open, significantly reducing outward seaweed movement (McManus et al. 2014). For simplicity, we assume that the seaweed velocity is zero when the grasper is open. Thus, instead of directly simulating the full equations of motion (see Appendix B) we use the reduced system

$$\frac{dx_r}{dt} = \frac{F_{\text{musc}}}{b_r}, \tag{16}$$

$$\frac{dx_{\text{sw}}}{dt} = 0 \tag{17}$$

when the grasper is open, and

$$\frac{dx_{\text{sw}}}{dt} = \frac{dx_r}{dt} = \frac{F_{\text{musc}} + F_{\text{sw}}}{b_r + b_{\text{sw}}} \tag{18}$$

when the grasper is closed.

It is entirely possible that the system is effectively quasi-static, and that positional forces dominate over viscous forces, but this formulation does not assume that from the outset.

Note that, in this formulation, sufficiently strong seaweed forces could pull the grasper out of its operating range $[0,1]$. To prevent this (unrealistic) situation from occurring, we impose boundary conditions limiting the motion of the grasper at $x_r = 0$ and $x_r = 1$, similar to those imposed on the neural variables.

3.3 Proprioceptive input

Proprioceptive neurons detect the position of and forces within the animal’s body. These mechanoreceptors can take many forms, from the muscle spindles and golgi tendon organs of vertebrates to the muscle organs seen in crustaceans to the S-channel expressing neurons seen in mollusks (Vandorpe et al. 1994). Rather than model these in detail, we have assumed that, as a function of the position of the grasper, the proprioceptive sensory neurons will create a net excitation or inhibition of each neural pool. For simplicity we have used a linear relation for this proprioceptive input as a function of position,

$$g_i(x_r) = (x_r - S_i)\sigma_i, \tag{19}$$

where $x_r \in [0, 1]$ is the position of the grasper, S_i is the position where the net proprioceptive input to the i th neural pool is zero, and $\sigma_i \in \{-1, 1\}$ is the direction of proprioceptive feedback for the i th neural pool. This term corresponds to the term $g(a, x)$ in the general framework described by Eq. (1), where its strength is scaled by the parameter ϵ . In

this case, however, the proprioceptive input does not depend upon \mathbf{a} , and so we write it simply as $g_i(x_r)$.

3.4 Noise

All biological systems are subject to noise, and as we will show, this can have important effects on the dynamics. Typical examples of noise in a neural context would include the small fluctuations caused by opening and closing of ion channels (known as channel noise; White et al. 2000; Goldwyn and Shea-Brown 2011), the variable release of neural transmitter vesicles, and stochastic effects from small numbers of molecules in second messenger systems. One can also treat parts of the system that we are not including in the model as “noise” (Schiff 2012), such as small variations in sensory input from the environment with a mean of zero.

We model this noise as a 3-dimensional Wiener process of magnitude η (i.e. white noise). This form of noise arises naturally when the noise is created by many small identical independent events with finite variance, such as channels opening and closing. Although most biological noise is bandwidth limited, the higher frequencies of the noise are filtered out by the dynamics of the model and can thus be ignored. Noise is added to the neural state variables a_i but is assumed to be negligible for the mechanical state variable x_r . For simulations in which noise is used, we thus replace the ordinary differential Eq. (3) with the stochastic differential equation

$$d\mathbf{a} = (f(\mathbf{a}, \mu) + \epsilon g(x_r)) dt + \eta dW_t, \tag{20}$$

where W_t is a three-dimensional Wiener process.

3.5 Parameter changes used for the limit cycle simulations

As mentioned in Section 3.1, the isolated neural dynamics (i.e. when $\epsilon = 0$) exhibits a stable heteroclinic cycle when $\mu = 0$, and a stable limit cycle for small positive values of μ .¹ Upon increasing μ from zero, one observes a qualitative change in dynamics in the fully coupled system ($\epsilon > 0$) at a critical value, μ_{crit} , which divides the parameter space into distinct regimes. We explore the differences between these two dynamical regimes in detail below. Although the central system exhibits a limit cycle in both regimes, the sensitivity of the oscillation to sensory feedback changes dramatically above versus below μ_{crit} . We call the $\mu < \mu_{\text{crit}}$ regime the “heteroclinic” regime because here the interplay of proprioceptive feedback with the underlying stable heteroclinic channel architecture governs the timing of the oscillation.

¹For sufficiently large values of μ , the intrinsic excitation overwhelms the mutual inhibition between the pools and all of the pools become tonically active via a supercritical Hopf bifurcation. This tonic activity does not produce ingestive behavior in our model, so we will not examine it further in this paper.

In contrast, for $\mu > \mu_{\text{crit}}$, the timing of the cycle is largely unaffected by proprioceptive feedback; we call the latter the “limit cycle” regime.

Several of the results described later involve comparing representative examples of systems in each of the two regimes. As we will describe in Section 5.2, without additional tuning of the parameters, the limit cycle performs much more poorly than the heteroclinic regime. For the limit cycle models, we thus change a small number of parameters, specifically, the neural time constant τ_a and the maximum muscle activation u_{max} . We also perform a phase dependent adjustment of timing by replacing the neural time constant τ_a with the following activity-dependent time scaling function

$$\tau_a(\mathbf{a}) = (1 + \boldsymbol{\alpha} \cdot \mathbf{a})\beta. \quad (21)$$

Here β is a scalar parameter representing a uniform adjustment in the speed of the trajectories (analogous to the previous constant τ_a), and $\boldsymbol{\alpha}$ is a vector parameter representing an activity-dependent scaling of the speed. Note that this change affects the timing but not the location of the trajectories in space in the isolated neural dynamics.

4 Materials and methods

Predictions of the model were tested using data from intact animals, semi-intact preparations in which all but feeding proprioceptive input had been removed (the suspended buccal mass), and preparations from which all sensory input had been removed (the isolated cerebral and buccal ganglia). Adult *Aplysia californica* were obtained from Marinus Scientific, Long-Beach CA, USA. The animals were housed in aerated 50 gallon aquariums at 16°C with a 12 hour light/dark cycle and were fed 0.5 g of dried laver every other day. Animals were presented with seaweed to test feeding behavior before use, and all animals used generated bites at 3 to 5 second intervals when tested.

4.1 Intact animals

Details of the recording methods for intact animals are described in Cullins and Chiel (2010). Briefly, animals from 350 g to 450 g were anesthetized by injecting 30 % of the animal’s mass of isotonic (0.333 molar) magnesium chloride solution into the hemocoel. Hook electrodes were then surgically implanted and attached to the I2 muscle, the radular nerve (RN), buccal nerve 2 (BN2), and buccal nerve 3 (BN3). The animals were allowed to recover, and they were then presented with 5 mm wide seaweed strips to elicit swallowing patterns. Video and EMG/ENG were recorded simultaneously to capture the behavior corresponding to the feeding motor patterns. Electrical recordings were made

using an A-M Systems model 1700 amplifier with a 10-1000 Hz band-pass filter for EMG and a 100-1000 Hz bandpass filter for the ENG recordings, and they were captured using a Digidata 1300 digitizer and AxoScope software (Molecular Devices).

4.2 Suspended buccal mass preparation

The methods used for the suspended buccal mass are described in McManus et al. (2012). Briefly, animals from 250 g to 350 g in weight were anesthetized by injecting 50 % of the animal’s mass of isotonic magnesium chloride into the hemocoel. The buccal mass and attached buccal and cerebral ganglia were then dissected out and placed in *Aplysia* saline (460 mM NaCl, 10 mM KCl, 22 mM MgCl₂, 33 mM MgSO₄, 10 mM CaCl₂, 10 mM glucose, 10 mM MOPS, pH 7.4-7.5). Hook electrodes were attached to the I2 muscle, RN, BN2, BN3, and branch a of BN2 (BN2a). The buccal mass was then suspended via sutures through the soft tissue at the rostral edge and the two ganglia pinned out behind it, with the cerebral ganglia placed in a separate chamber isolated from the main chamber using vacuum grease. To elicit ingestive patterns, the *Aplysia* saline in the chamber containing the cerebral ganglion was changed to a solution of 10 mM carbachol (Acros Organics) in *Aplysia* saline. Electrical recordings were made using an A-M Systems model 1700 amplifier with a 10-500 Hz band-pass filter for EMG and a 300-500 Hz bandpass filter for the ENG recordings, and they were captured using a Digidata 1300 digitizer and AxoGraph software (Axon Instruments).

4.3 Isolated buccal ganglion

The methods used for the isolated ganglia are described in Lu et al. (2013). Briefly, the animal was euthanized and the buccal mass and buccal and cerebral ganglia dissected out as described for the suspended buccal mass. The ganglia were then dissected away from the buccal mass along with a small strip of I2 attached to the I2 nerve, and the ganglia was pinned out in a two-chambered dish lined with Sylgard 184 (Dow Corning), with a vacuum grease seal separating the solution in the chamber with the cerebral ganglion from that in the chamber with the buccal ganglion. Suction electrodes were attached to BN2, BN3, RN, and the excised strip of the I2 muscle. For ingestive patterns, a 10 mM carbachol solution was applied to the chamber containing the cerebral ganglion. Electrical recordings were made using an A-M Systems model 1700 amplifier with a 10-500 Hz band-pass filter for EMG and a 300-500 Hz bandpass filter for the ENG recordings, and they were captured using a Digidata 1300 digitizer and AxoGraph software (Axon Instruments).

4.4 Data analysis

Selection of patterns for analysis varied by preparation. For the intact animal, patterns were considered swallows if the video showed the animal grasping the seaweed throughout the pattern and the net movement of the seaweed was inward; other behaviors such as bites and rejections were not studied for this paper. For the suspended buccal mass and isolated ganglia, patterns were used near the middle of the experimental session following carbachol application, as the patterns tend to be more distorted when carbachol is first added and late into the application as the behavior slows.

Onsets and offsets of activity in the I2 muscle EMG were identified based on the onset and offset of high frequency firing. Activity of I3 was identified based on the activity of the three largest units on the buccal nerve 2 ENG, which have previously been identified by our lab as B3, B6, and B9 (Lu et al. 2013). A subset of the burst onset and offset timings were independently identified by a second researcher to verify inter-rater reliability.

4.5 Numerical methods

The stochastic differential equations were simulated in C++ using an explicit order two weak scheme with additive noise, described in Kloeden and Platen (1992). If the stochastic differential equation is expressed in vector form as

$$dy_t = A(y_t) dt + B(y_t) dW_t, \tag{22}$$

this scheme is described by the following recurrence relationship:

$$\tilde{y}_{n+1} = y_n + A(y_n)h + B(y_n)\Delta W_n, \tag{23}$$

$$y_{n+1} = y_n + \frac{1}{2}(A(\tilde{y}_{n+1}) + A(y_n))h + B(y_n)\Delta W_n. \tag{24}$$

Here h is the length of a time step and ΔW_n is a Weiner increment (a vector of pseudo-random numbers from a Gaussian distribution with mean zero and variance h). Note that in the deterministic case this reduces to the Heun method (Kloeden and Platen 1992).

Random numbers for the Wiener increments were generated using a Mersenne twister with a period of $2^{19937} - 1$ (Matsumoto and Nishimura 1998). A time step of size 10^{-3} was used. This was verified to be sufficiently small by simulating the model with default parameters and seeing a change in period of less than 30 parts per million (from 4.02704 to 4.02693) when the step size was changed from 10^{-3} to 10^{-4} . Onsets and offsets of bursts were determined by when the activity of the next neural pool rose above the previous one (i.e. $a_{i+1} > a_i$), and were linearly interpolated between time steps to improve accuracy.

5 Results

5.1 Endogenous excitation vs. sensory feedback

The marine mollusk *Aplysia* must adapt to the changing forces imposed on it by the stipe of seaweed it is attempting to consume. These forces can vary considerably during feeding; a stipe of seaweed might initially present very little resistance, but accumulated elastic forces in the seaweed will grow as the animal pulls against the holdfast, and tidal forces can present a sudden load with little warning.

The ability of *Aplysia* to respond adaptively to mechanical loads during feeding depends on the balance between the intrinsic excitability of the isolated nervous system and the strength of proprioceptive feedback. Therefore, we first systematically explored how the interplay of proprioceptive feedback and intrinsic excitability affects the response of the model to a range of mechanical loads. In the equations governing the neural state variables (see Appendix A) the endogenous excitation (μ) is added to the proprioceptive feedback, which is scaled linearly by the parameter ϵ .

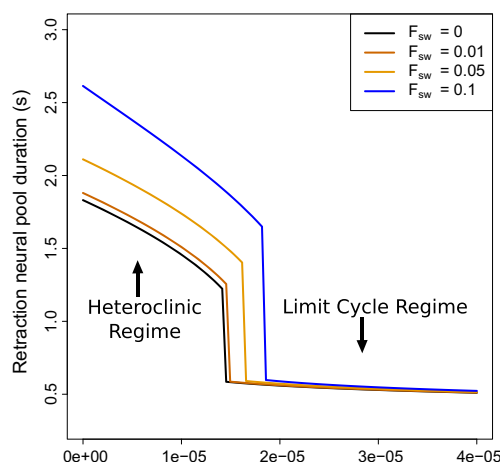


Fig. 4 Retraction phase duration is sensitive to sensory feedback when intrinsic neuronal excitability is low, but not when it is high. Across a range of forces, the duration of the retraction neural pool activity undergoes a sharp, qualitative change at a critical value of μ . Thus, we divide the parameter space into “heteroclinic” (low μ , below the transition point) and “limit cycle” (high μ , above the transition point) regimes. This transition is present even at zero force (*black line*), but the critical μ value is larger for greater forces. Below the transition (small μ), the retraction duration is longer, and the duration increases significantly with increasing seaweed force, as can be seen by comparing the *black curve* ($F_{sw} = 0$) to the *blue curve* ($F_{sw} = 0.1$). For large μ above the transition, the retraction duration is shorter and largely unaffected by the applied seaweed force. This implies that the model is capable of operating in two dynamical regimes. As a shorthand, throughout the paper we refer to μ values below the transition point as belonging to the “heteroclinic” regime, and μ values above the transition as belonging to the “limit cycle” regime

Thus we fixed the parameter controlling the strength of proprioception (ϵ), and observed the dynamics of the model across a range of endogenous excitation levels (μ) for several different applied loads (F_{sw}). We focused on retraction duration as a way of measuring the responsiveness of the system to load, since in the retraction phase the grasper is closed on the seaweed and the muscles are actively countering the seaweed force. Longer retractions allow the muscles to build up more force and thus more effectively counter the applied load. Figure 4 shows the activity duration in seconds of the retraction neural pool a_2 , which drives the retractor muscle I3, across a range of μ values. Curves for several values of the resisting seaweed force F_{sw} are shown, ranging from $F_{sw} = 0$ to $F_{sw} = 0.1$. Here all other parameters are held constant at their default values as listed in Appendix C, and for each curve, only μ is systematically varied.

Figure 4 indicates that, depending on the level of endogenous excitation, the response to mechanical load operates in two distinct dynamical regimes. First, note that in each curve there is a sharp transition at some nonzero, critical μ value, which becomes more dramatic for greater mechanical loads. For μ values below the transition point, the retraction

phase is longer and increases with higher seaweed force. In contrast, for μ values above the transition point, the retraction phase is significantly shorter and is only weakly affected by the seaweed force. Also note that the critical μ value increases as the seaweed force is increased.

The existence of this transition allows us to separate the parameter space into two distinct regimes. The first of these regimes, which corresponds to the range of μ values below the transition point, we refer to as the “heteroclinic” regime. In the heteroclinic regime, the system is sensitive to mechanical load. We refer to the range of μ values above the transition point as the “limit cycle” regime. In this second regime, the system is no longer sensitive to mechanical load.

To understand this qualitative change, consider the dynamics on either side of the transition for the fixed force $F_{sw} = 0.05$. For this force value, the sharp change occurs at approximately $\mu_{crit} = 1.7 \times 10^{-5}$. Figure 5 shows example trajectories for the μ values $\mu_1 = 1.6 \times 10^{-5}$ (heteroclinic regime, left) and $\mu_2 = 1.8 \times 10^{-5}$ (limit cycle regime, right), respectively, as examples of the dynamics on either side of the transition. All other parameters are kept fixed. The top

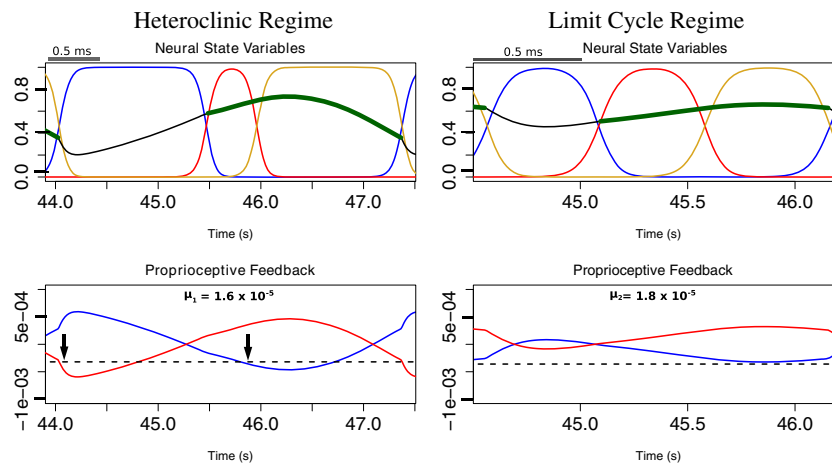


Fig. 5 A small change in endogenous excitation near the critical value of μ switches the dynamical regime. *Top panels* The trajectories of the state variables over a single cycle, for μ values just below and above the transition point, when $F_{sw} = 0.05$. The *top left panel* shows trajectories for the heteroclinic regime ($\mu_1 = 1.6 \times 10^{-5}$), whereas the *top right panel* shows trajectories for the limit cycle regime ($\mu_2 = 1.8 \times 10^{-5}$). In both plots, the a_0 (protraction open), a_1 (protraction closing) and a_2 (retraction) variables are shown in blue, red, and yellow, respectively. The position of the grasper is plotted in black, with 1 corresponding to full protraction and 0 to full retraction. The thick portion of the curve indicates where the grasper is closed. The limit cycle regime trajectory has a shorter cycle period relative to the heteroclinic regime trajectory (note 0.5 ms scale bars left and right), and this difference is primarily manifested in durations of the a_0 and a_2 neural pools. *Bottom panels* The proprioceptive inputs to the a_0 (blue)

and a_1 (red) neural pools, for the heteroclinic regime (left), and the limit cycle regime (right). The dashed black lines show the constant values $-\mu_1/\tau_a$ (left) and $-\mu_2/\tau_a$ (right) for reference. Note that in the heteroclinic regime example (left), the proprioceptive feedback curves cross the horizontal line at $-\mu_1/\tau_a$. In this regime, sensory feedback is able to overcome the neural dynamics and “pin” the neural state variables to one of the fixed points until the appropriate mechanical state is reached. In contrast, in the limit cycle regime example (right), the proprioceptive feedback curves never cross the line at $-\mu_2/\tau_a$. In this regime, the proprioceptive input never exceeds the intrinsic neural dynamics and thus has only a weak effect on the cycle timing. Note that in the heteroclinic regime (left) the grasper is able to retract more fully, which both increases the proprioceptive feedback and allows for greater inward seaweed movement

panels on both the left and right show the time courses of the a_0 (blue), a_1 (red), and a_2 (yellow) neural state variables, and the position of the grasper (black), for a single cycle. The bottom panels on either side show the total proprioceptive input (given by the term $\epsilon(x_r - S_i)\sigma_i$ in the equations) to the a_0 (blue) and a_1 (red) neural pools, along with the constant quantity $-\mu/\tau_a$ (black, dashed line).²

We found that the transition between the two regimes is governed by the relative balance of endogenous excitation and inhibitory proprioceptive feedback, in the following sense. Consider initial conditions for which the neural activity vector lies on one of the three lower-bound planes Π_i (see Section 3.1). Then the i^{th} component a_i equals zero, and has rate of change $\dot{a}_i = (\mu/\tau_a) + \epsilon g_i(x)$, where g_i is the i^{th} component of the proprioceptive feedback vector g . If the full system has a periodic solution for which the mechanical component $\mathbf{x}(t)$ satisfies $\mu/\tau_a > |\epsilon g(\mathbf{x}(t))|$ for all t , then the flow of the neural subsystem at the boundary Π_i is always transverse and inwards. That is, the periodic neural trajectory $\mathbf{a}(t)$ corresponding to such a periodic mechanical trajectory $\mathbf{x}(t)$ will remain in the interior of the unit cube, and the boundary conditions on \mathbf{a} will never need to be enforced. In this case the behavior of the model retains the character of a typical limit cycle system.

On the other hand, if there is a range of t for which $\mathbf{x}(t)$ satisfies $-\mu/\tau_a > \epsilon g_i(x)$, then it is possible that the neural components $\mathbf{a}(t)$ could collide with the plane Π_i , requiring the boundary conditions to be enforced. Empirically, as we vary μ , we find that the system behavior changes dramatically when any of the proprioceptive terms $\epsilon g_i(x_r(t))$ crosses the value $-\mu/\tau_a$ from above. It is at just such a value of μ that the system enters the heteroclinic-dominated regime.³

Figure 5 illustrates this change in behavior. In the heteroclinic regime (left), the proprioceptive feedback to the a_0 and a_1 neural pools both cross the line at $-\mu_1/\tau_a$. When this occurs, the proprioceptive feedback provides sufficiently strong inhibition to overcome the endogenous excitation (μ_1/τ_a), which suppresses the activity of that neural pool. Since the pools are inhibitorily coupled, suppressing the activity of the pool that is next to activate removes

inhibition to the currently active pool. This allows the activity of the currently active pool to reach a maximum, pushing the neural state variables close to one of the fixed points and thereby halting progression of the neural dynamics through the cycle. When the neural variables are held in place by the proprioceptive feedback, the dynamics are driven entirely by the slow mechanical variables. The cycle will therefore only advance when the grasper reaches the appropriate position, such that the proprioceptive input no longer counters the endogenous excitation. Since progress through the cycle depends upon the state of the mechanical variables, the system is highly sensitive to mechanical forces affecting the position of the grasper.

In contrast, in the limit cycle regime (Fig. 5, right), the proprioceptive input cannot overcome the greater endogenous excitation, resulting in markedly different dynamics. As illustrated in the bottom right panel of Fig. 5, in this regime the proprioceptive inputs never cross the line at $-\mu/\tau_a$ and thus never dominate the intrinsic neural dynamics. Consequently, progression through the cycle occurs regardless of the position of the grasper. This leads to more limit-cycle-like behavior and a significantly reduced sensitivity to mechanical load. Note that in this regime, the system has a considerably shorter cycle period, since the transition between phases is driven by the fast neural variables rather than the slow mechanical variables.

These observations also provide insight into both the increase in retraction durations and the larger critical values of μ at higher forces. In the heteroclinic regime, proprioceptive feedback will suppress the onset of the protraction pool until the grasper is sufficiently retracted. With increased mechanical load, retraction occurs more slowly, since the slow muscles must build up a sufficient amount of force to overcome the resisting seaweed force. This slower retraction extends the duration of the inhibitory proprioceptive input to the protraction neural pool, thereby delaying the onset of protraction and extending the retraction phase. The critical μ value increases at higher forces because the increased force produces stronger proprioceptive feedback during the protraction closing phase, which can overcome higher levels of endogenous excitation.

Thus, by systematically examining the balance between sensory input and endogenous excitation, we see that the model can operate in two different regimes: 1. A heteroclinic regime, in which the proprioceptive feedback can dominate and push the neural state variables very close to the fixed points (resulting in long dwell times near the fixed points), and 2. a limit cycle regime, in which the intrinsic neural activity is sufficiently strong that it always dominates the proprioceptive feedback, resulting in generic limit-cycle-type dynamics.

²Note that in Equation 4, the endogenous excitation μ is scaled by the neural time constant τ_a . Thus the total endogenous excitation which must be overcome by the proprioceptive feedback is $\frac{\mu}{\tau_a}$. This occurs when the sum of the proprioceptive term and $\frac{\mu}{\tau_a}$ is less than zero, and thus we plot the constant quantity $-\frac{\mu}{\tau_a}$ in the bottom panels of Fig. 5 as a reference. Note that in both cases the proprioceptive input to the a_2 neural pool never crosses the threshold $-\mu/\tau_a$, and thus is not plotted.

³In general, global bifurcations in non-smooth systems can be difficult to analyze (Di Bernardo et al. 2008; Makarenkov and Lamb 2012). A more detailed analysis focusing on the bifurcation structure of the fully coupled system lies beyond the scope of this paper.

5.2 Comparing the performance of the limit cycle regime to the heteroclinic regime

We have seen that the model can operate in one of two distinct dynamical regimes, with the primary distinction being that in one regime (the heteroclinic regime), the neural dynamics are sensitive to proprioceptive input and mechanical load, while in the other (the limit cycle regime), they are not. Next we ask whether the enhanced sensitivity to load seen in the heteroclinic regime confers any functional or behavioral advantages. We therefore explore the efficacy of the limit cycle and heteroclinic regimes in the ingestion of seaweed over a range of resisting forces on the seaweed. As a representative example of a system falling within the heteroclinic regime, we ran the model with the very small but non-zero μ value of 10^{-9} . We do not set this parameter identically equal to zero since for this (and only this) value the isolated neural dynamics possess a heteroclinic *cycle* rather than a stable heteroclinic channel. As an example of the system in the limit cycle regime, we ran the simulation for the much larger μ value of 10^{-3} . These choices ensure that the two examples will lie safely on either side of the transition point across all of the parameter ranges we explore.

Although the heteroclinic regime model can be switched to the limit cycle regime by increasing the intrinsic excitability μ , as shown in Fig. 6 (top line: heteroclinic regime, $\mu = 10^{-9}$; bottom line: limit cycle regime,

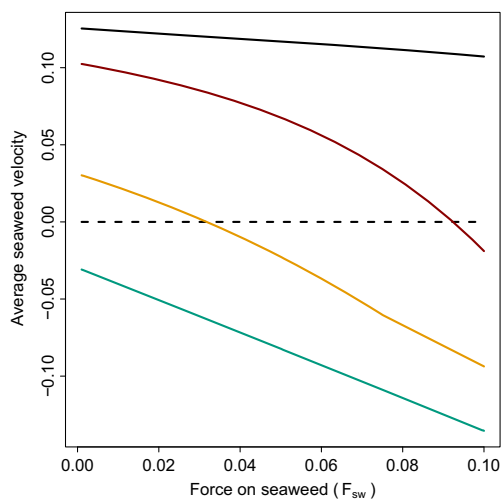


Fig. 6 The limit cycle regime example produced by changing intrinsic neural excitability (μ) alone performs much more poorly than the heteroclinic regime, but the limit cycle regime’s performance can be improved by adjustments in timing. *Top black line* heteroclinic regime. *Lower green line* limit cycle regime example produced by only changing μ . *Orange line*, second from bottom: limit cycle regime example produced by changing μ and τ_a , which controls the overall cycle duration. *Red line*, third from bottom: limit cycle regime example produced by changing μ and replacing the constant τ_a with the function $\tau_a(\mathbf{a}) = (1 + \alpha \cdot \mathbf{a})\beta$, thus allowing the limit cycle regime to spend similar times to the heteroclinic regime at different phases of the motor pattern

$\mu = 10^{-3}$; all other parameters fixed), the resulting model is unable to effectively ingest seaweed. We thus attempt to tune the parameters for the limit cycle regime to make it more effective and more comparable to the heteroclinic regime. We use the behavior of the heteroclinic regime under a light seaweed load ($F_{sw} = 0.01$) to guide our parameter changes. Under these conditions, the heteroclinic regime ingests seaweed at a rate of $0.125/s$, but the limit cycle regime (with changes to μ only) *egests* seaweed at a rate of $0.03/s$ (i.e. the seaweed is pushed out more than it is pulled in).

There are a number of reasons why the limit cycle regime is less effective at ingesting seaweed. The increase in μ dramatically decreases the time spent near the saddles without increasing the time spent moving between saddles; as a result, the period of the neural pattern decreases from $4.45s$ to $0.99s$. To compensate for this change, we increased the time scaling constant τ_a for the limit cycle regime so that its cycle period matched that of the heteroclinic regime. This adjustment increases the efficacy of the limit cycle regime to ingest at a rate of $0.030/s$; a similar improvement is seen across a range of loads as shown in Fig. 6, second line from the bottom.

The next obvious cause of the lower efficiency of the limit cycle regime is the approximately equal length of time each neural pool is active; with the changes to μ and the constant τ_a , each pool is active for 1.49 , 1.46 , and 1.50 seconds for protraction open, protraction closing, and retraction closed, respectively, whereas in the heteroclinic regime, protraction closing ($0.49s$) is much shorter than protraction open and retraction closed ($2.08s$ and $1.88s$). These differences in how long each neural pool is active are likely to be due to differences in sensory responsiveness, which we will explore in Section 5.3. In general, a limit cycle could spend different amounts of time in each region of the pattern without requiring dependence on sensory input. To illustrate this point, we adjust the timing of the limit cycle by making τ_a activity-dependent, as described in Equation 21, setting β equal to our previous constant τ_a and adjusting the parameter vector α to make the duration of activity match that seen in the heteroclinic regime with the test seaweed load. This increases the efficacy of the limit cycle to $0.102/s$, and again improves the performance of the limit cycle regime across a range of loads as shown in Fig. 6, third line from the bottom.

Despite these changes to the intrinsic neural dynamics, the limit cycle is still less effective than the heteroclinic regime. One reason for this remaining deficit is that the sharp transitions in the heteroclinic regime may provide faster activation of the muscles than the more gradual onset and offset of activity in the limit cycle. As shown in Fig. 7, this slower activation and deactivation can be compensated for by increasing the maximum activation of the muscle (or,

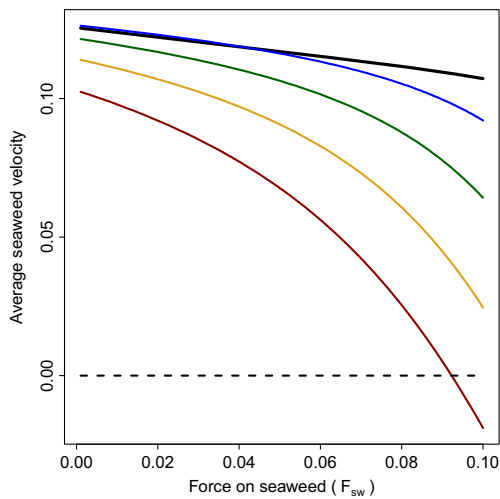


Fig. 7 Increasing the maximum muscle activation allows the system in the limit cycle regime to perform as well as that in the heteroclinic regime, over a range of forces. *Black line* heteroclinic regime. *Red line, yellow line, green line, and blue line*: limit cycle regime with timing changes and 1, 1.2, 1.4, or 1.6 times the maximum muscle activation, respectively

equivalently, the cross section of the muscle) u_{max} . Increasing u_{max} by a factor of 1.6 results in a rate of ingestion of 0.126, which is slightly higher than the efficacy of the heteroclinic regime. Note that, as shown in the figure, even with higher values of u_{max} , the heteroclinic regime is more effective than the limit cycle regime when the mechanical load due to the seaweed increases.

Although increasing the maximum muscle activation allows the limit cycle regime to match or even exceed the efficacy of the heteroclinic regime over a range of

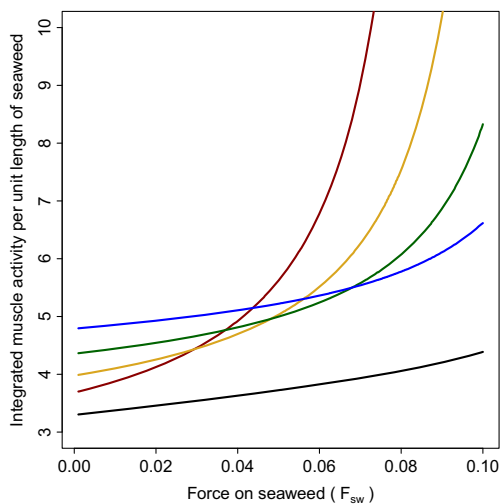


Fig. 8 Increased muscle activation in the limit cycle regime comes at a metabolic cost (see Eq. (25)). *Black line* heteroclinic regime. *Red line, yellow line, green line, and blue line*: limit cycle regime with timing changes and 1, 1.2, 1.4, or 1.6 times the maximum muscle activation, respectively

loads, this change has a metabolic cost for the animal. To a first approximation, the energetic cost of contraction is proportional to the force generated by the muscle (Sacco et al. 1994). Thus, under the model’s assumption that we are in the linear regime of the force-activation curve, the energetic cost of contraction is also proportional to the activation of the muscle. In Fig. 8 we show the energetic cost, in the form of integrated muscle activation over time, per length of seaweed ingested. Assuming the system has reached steady-state, this is

$$\frac{\int_0^T \sum_i u_i(t) dt}{x_{sw}(0) - x_{sw}(T)}, \tag{25}$$

where T is the period of the behavior. Note that even at low loads, the limit cycle regime pays a higher metabolic cost per unit length of seaweed ingested.

The behavior of the limit cycle regime is also mechanically less efficient at higher loads. In Fig. 9, we show the mechanical work done by the muscles per unit length of seaweed ingested,

$$\frac{\int_0^T F_{musc}(s) \frac{dx_T}{dt} \Big|_{t=s} ds}{x_{sw}(0) - x_{sw}(T)}. \tag{26}$$

Note that the limit cycle regime is able to remain mechanically efficient over a larger range of loads when the muscles are strengthened, but the heteroclinic regime is still more mechanically efficient at higher loads than the limit cycle regime with muscles that are 1.6 times stronger. We will explore the differences in behavior that lead to these effects in the next section.

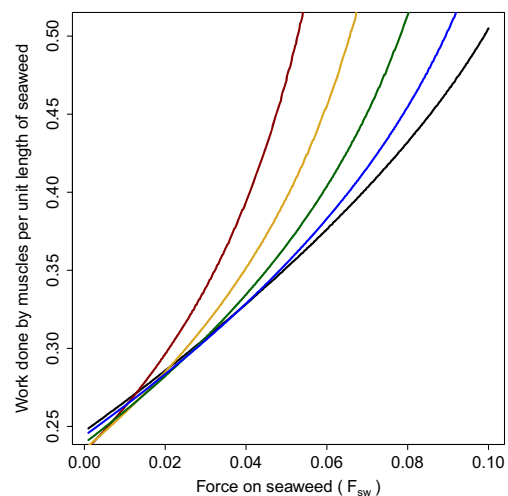


Fig. 9 With higher loads, the system in the limit cycle regime is less efficient than in the heteroclinic regime, and does more mechanical work (Eq. (26)) for a given amount of seaweed ingested. *Black line* heteroclinic regime. *Red line, yellow line, green line, and blue line*: limit cycle regime with timing changes and 1, 1.2, 1.4, or 1.6 times the maximum muscle activation, respectively

5.3 Mechanisms of adaptation to load

How do the two architectures adapt to changes in mechanical load? In Fig. 10, we can see the changes between low and high seaweed forces. In the limit cycle regime, the time course of neural activation is very similar under both high ($F_{sw} = 0.1$) and low ($F_{sw} = 0.01$) load conditions. As a result, the forces in the high-load condition dramatically reduce the distance that the seaweed

is pulled inward before the grasper releases the seaweed (thick green line). Note that once the seaweed is released, the retraction force on the grasper is no longer opposed, causing a rapid retraction. In the heteroclinic regime, by comparison, we can see that the neural pool involved in retraction (yellow) increases its duration of activity. The resulting long retraction allows the animal to draw in more seaweed by allowing the muscles to exert a greater peak force.

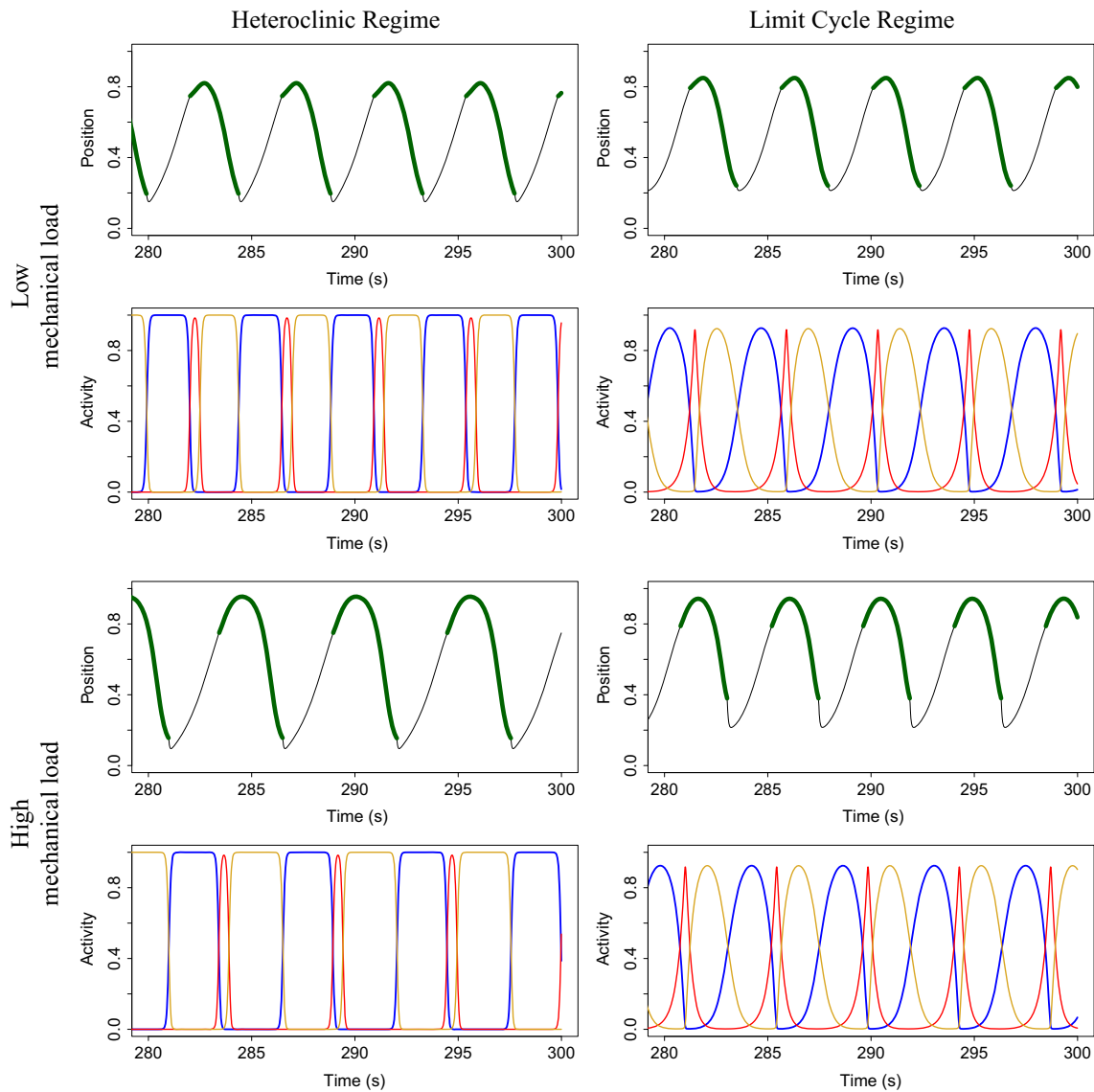


Fig. 10 Forces on seaweed can selectively prolong the retraction phase of the heteroclinic regime, but have little effect on the limit cycle regime. *Black and green lines* show the position of the grasper, with the thick green sections showing the positions when the grasper is closed on the seaweed and the black sections showing the positions when the grasper is open. The *blue, red and yellow lines* show the activity of the protraction open, protraction closing, and retraction closed neural pools, respectively. The mechanical load, F_{sw} was increased from 0.01 to 0.1. The positions of the grasper are similar

for both the heteroclinic regime and the limit cycle regime when there is little load. Note that the duration of retraction closed (yellow) increases substantially in the heteroclinic regime under high load, resulting in a stronger retraction while holding the seaweed; this is not true in the limit cycle regime under load. The sensitivity to load in the heteroclinic regime is due to sensory feedback counteracting the endogenous excitation and delaying the onset of the protraction neural pool, as demonstrated in Figs. 4 and 5

This difference in response is consistent with our observations in Fig. 4 that, in the heteroclinic regime, the system compensates for higher loads by increasing the duration of the retraction neural pool activity, whereas in the (untuned) limit cycle regime, the system is largely insensitive to seaweed forces. To examine more systematically how the tuned limit cycle regime responds to changes in force, in Fig. 11 we plotted the retraction neural pool duration across a range of forces for both the heteroclinic and limit cycle regime examples. Here we see clearly that the heteroclinic regime example systematically increases retraction duration in response to increasing force, whereas the limit cycle regime example is insensitive to changes in load, even when the time constants and muscle activation parameters have been tuned.

The mechanisms of these changes in timing can be seen in more detail in Fig. 12. In both the heteroclinic and limit cycle regimes, the trajectory is moved only a small distance by sensory input. In the case of the limit cycle regime, the new trajectory passes through a very similar region of phase space as the unperturbed trajectory, and thus the timing of the oscillation does not change very much. In contrast, in the heteroclinic regime, the small perturbation moves the trajectory near the saddle point where the flow decreases rapidly even over these short distances. During retraction, the trajectory passes closer to the saddle where the flow is very small; thus it spends longer in this region.

It is natural to ask whether the intact behaving animal employs similar strategies. Because it is difficult in the intact animal to assess the dynamic forces generated by seaweed bunching up in the buccal cavity as seaweed is

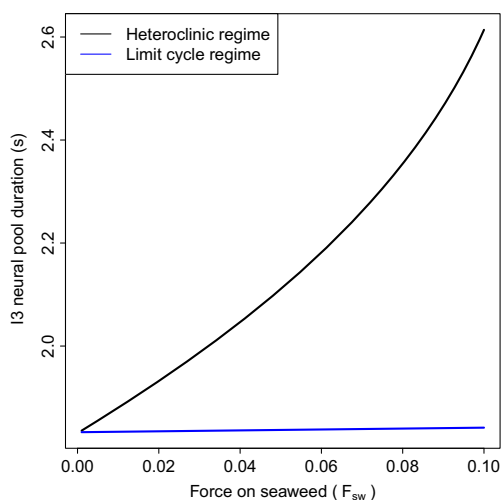


Fig. 11 In the heteroclinic regime (black line, $\mu = 10^{-9}$), the system reacts to increasing the seaweed force by lengthening the duration of the retraction neural pool activity. In contrast, retraction duration in the limit cycle regime example (blue line, $\mu = 10^{-3}$) is relatively insensitive to mechanical load, despite adjustments to the neural time constants and the maximum muscle activation parameter

ingested, we consider a simplified situation where a stiff elastic force is encountered during a swallow that prevents the seaweed from moving inward, such as the holdfast of the seaweed. We can create an analogous situation in the animal by feeding the animal a thin strip of seaweed and then holding the seaweed during a swallow to present a resisting force.

How do these strategies compare to those used by the animal itself? As shown in Fig. 13, when seaweed is held by the experimenter to prevent inward movement, the duration of retraction increases, although the duration of protraction does not appear to increase or decrease.

It is not surprising that an animal would behave in an adaptive manner to the behaviorally relevant task of consuming seaweed. If the dynamics of the central nervous system are heteroclinic regime-like, would this create any changes that would not be expected from a purely adaptive standpoint? There are two we will discuss here: the response to removal of proprioceptive and excitatory input, and the shape of the distribution of durations of components of the pattern.

The removal of sensory input and excitatory drive can be simulated by setting ϵ and μ equal to zero. For these parameters, the system possesses a true heteroclinic cycle, and in the absence of noise or intrinsic excitability the duration of patterns will grow without bound. In our preparations of the isolated buccal ganglia, we observed that the isolated neural system did possess a small but not zero amount of intrinsic excitability. Therefore we simulated this situation by setting μ equal to a very small but non-zero value ($\mu = 10^{-30}$). Note also that the addition of noise could also produce oscillations in the pure heteroclinic cycle, leading to long, but still finite, cycle times. In Fig. 14 (left), we set μ to 10^{-30} to show that even a very small amount of constant excitation is sufficient to prevent the heteroclinic cycle from becoming “stuck” in one of the phases. In this case we see that the pattern duration is much longer than either the heteroclinic regime or limit cycle regime examples we have previously explored, which both have non-zero values of μ . Furthermore, this lengthening of the patterns depends upon the presence of an underlying heteroclinic architecture, since the slowing of the neural trajectory occurs due to the passage of the trajectory near a series of fixed points. If we reduce the influence of the fixed points by increasing μ , thereby making the system resemble a generic limit cycle (Fig. 14, right), then the removal of sensory input has very little effect (compare Fig. 14 top right and bottom right).

When sensory input is removed from the animal, does the duration of protraction and retraction increase as is seen in the heteroclinic regime, or remain about the same as is seen in the limit cycle regime? To investigate this, we examine

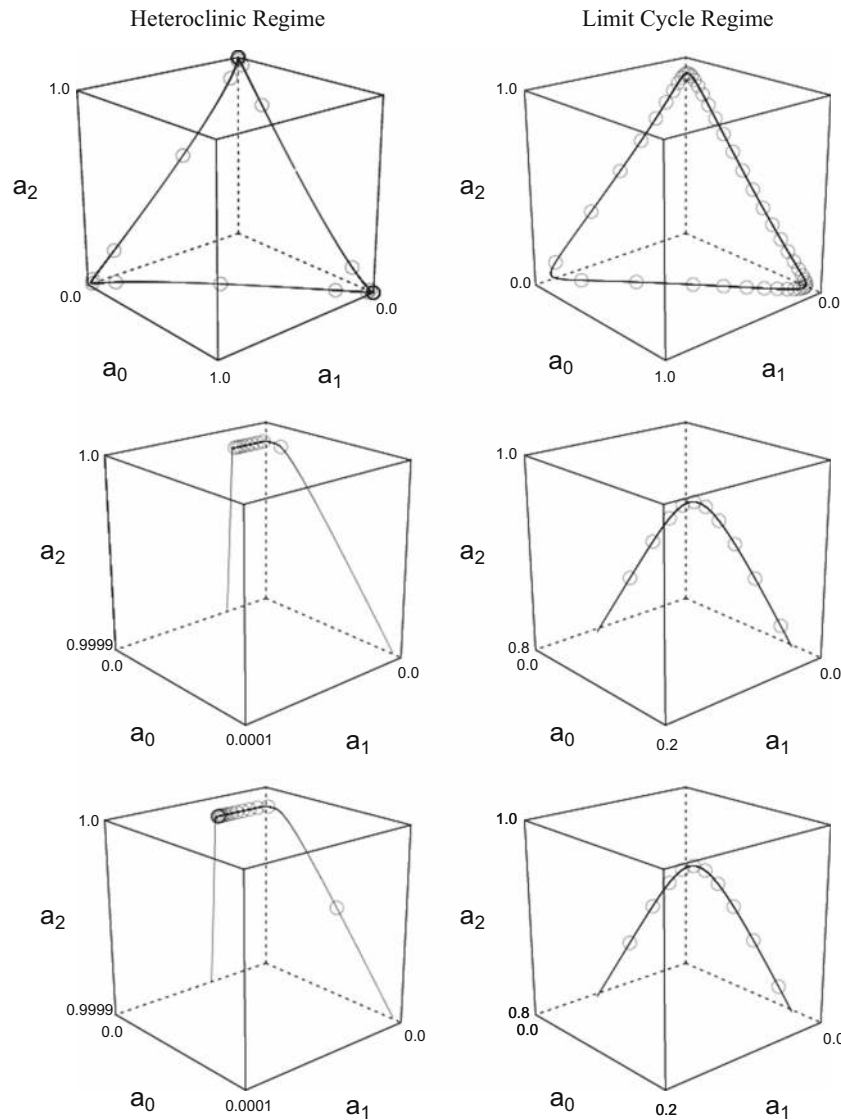


Fig. 12 A small change in the trajectory caused by sensory input can have a large effect on timing in the heteroclinic regime by pulling the trajectory closer to the saddle; the same magnitude of change has very little effect in the limit cycle regime. The upper row shows the trajectory of the neural variables in phase space with small load ($F_{sw} = 0.01$) for both the heteroclinic regime and the limit cycle regime. The circles represent points equally spaced in time (by 100 ms intervals) to show speed of the trajectory. Note that the trajectory of the heteroclinic regime spends almost all of its time near the saddles (at the corners of the triangle), whereas the limit cycle regime spends more time on the parts of the trajectory between two saddles. The second row contains a

magnification of the top corner of the trajectory (where the retraction-closed neural pool is most active) for the heteroclinic regime (left) and limit cycle regime (right) with the light mechanical load ($F_{sw} = 0.01$). The heteroclinic regime plots are magnified 10000 times, whereas the limit cycle plots are magnified 10 times. The third row shows trajectories for the same two examples after increasing the seaweed force ($F_{sw} = 0.1$). Note that in the limit cycle regime, the trajectory is largely unchanged. In the heteroclinic regime, however, the trajectory is pulled close to the saddle and spends a significantly longer amount of time in the retraction phase. This effect occurs only when sensory feedback is strong enough to overcome the endogenous excitation

two preparations of the animal with reduced sensory input and compared them to the intact animal. In the first preparation, the suspended buccal mass (McManus et al. 2012), the feeding apparatus and the ganglia controlling feeding are dissected out of the animal and suspended in a physiological saline. This preparation thus removes sensory input

from the lips, anterior tentacles, and other parts of the body, but not the proprioceptive feedback from the feeding apparatus itself. In the second preparation, the isolated ganglia, the feeding apparatus is also dissected away, leaving just the ganglia controlling feeding. As shown in Fig. 15, protraction (containing both the protraction open and protraction

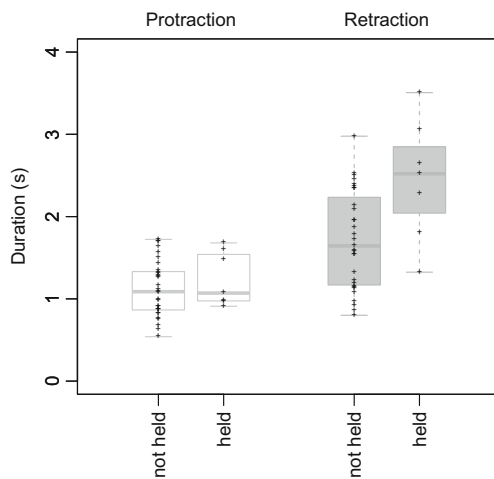


Fig. 13 When a force is applied to the seaweed *in vivo* (by holding the seaweed), the activity of the neurons involved in retraction (corresponding to retraction closed) is prolonged (*right*), while the activity of the protractor muscle (corresponding to the start of protraction open to the end of protraction closing) is not (*left*). Medians differ (Mann–Whitney test, $p = 0.013$). 30 unheld swallows and 7 held swallows were used from the same two animals. Results are similar if unheld swallows from all 6 animals are used (not shown, $p = 0.003$)

closing phases) and retraction (closed) both increase in duration from the intact animal to the suspended buccal mass, and increase further in duration from the suspended buccal mass to the fictive patterns of the isolated ganglia. Note that this increase in both protraction and retraction differs from the selective increase in retraction when the seaweed was held in Fig. 13, but matches the increase in both phases seen in the stable heteroclinic channel (Fig. 14).

When subject to small amounts of noise, the heteroclinic regime and the limit cycle regime show different forms of variability in timing. We illustrated this by running 10000 independent stochastic simulations of the model with low amplitude Gaussian noise (standard deviation $\eta = 10^{-4}$), for both the heteroclinic regime model and the limit cycle regime model. The retraction neuronal pool durations were collected from all simulations in both cases, and for each case we computed a distribution of duration times. The density functions were estimated using a kernel density estimator algorithm described in Silverman (1986). Each data point was convolved with a Gaussian kernel, and the resulting smoothed curves were summed to form a single function. This function was then normalized by dividing by the total area under the curve. The kernel bandwidth in each case was chosen based on the variance of the data (Silverman 1986).

The key result of simulations with noise, shown in Fig. 16, is that the distribution for the heteroclinic regime is significantly skewed compared to the more symmetric distribution for the limit cycle regime. In the limit

cycle regime, perturbations from the noise have very similar effects regardless of where they occur in the cycle, so, by the central limit theorem, their cumulative effect is approximately Gaussian in the limit of small noise.⁴ In contrast, in the heteroclinic regime, as described in Shaw et al. (2012), perturbations that occur while approaching the saddle can have much larger effects than perturbations that occur while leaving the saddle, so the central limit theorem does not apply. As predicted by Stone and Holmes (1990), this results in a distribution that is skewed to the right.

Using our *in vivo* preparation, we can measure the retraction duration during swallowing in intact *Aplysia*, and compare the resulting distribution to our simulation output. In Fig. 17, we see that the distribution of retraction durations is significantly skewed to the right, more closely resembling that seen in the heteroclinic regime of the model. The experimental distribution was computed via the same kernel density estimation procedure used for the simulated data.

6 Discussion

In this paper, we have examined a neuromechanical model of swallowing in *Aplysia* in two parameter regimes. In the first parameter regime, the internal neural dynamics drive the cycle in a manner similar to an idealized central pattern generator. In contrast, in the second parameter regime, which has dynamics more similar to those of a chain reflex, passage near saddle points leads to greater sensitivity to sensory inputs.

We have shown that the model operating within the limit cycle regime does not adapt as well to changing loads as the model operating within the heteroclinic regime, even when the durations of the cycle components have been tuned to be the same in both regimes (Figs. 6–9). We showed that part of this change is due to a prolongation of retraction allowing greater activation of the slow retractor muscles (Figs. 10, 11). We then showed that the animal itself appears to use the same strategy of prolonging retraction when faced with loads *in vivo* (Fig. 13).

We showed that, in the heteroclinic regime, the model could more accurately capture behaviors observed in experimental data than in the limit cycle regime, even for aspects of the behavior that do not convey an obvious evolutionary advantage. First, removal of sensory feedback and reduction of endogenous excitation resulted in

⁴In the limit cycle regime, the time spent passing through one part of the cycle can be approximated as the first passage time of a Brownian particle with drift, so the small noise assumption is important; the distribution will become skewed as the noise becomes large relative to the drift.

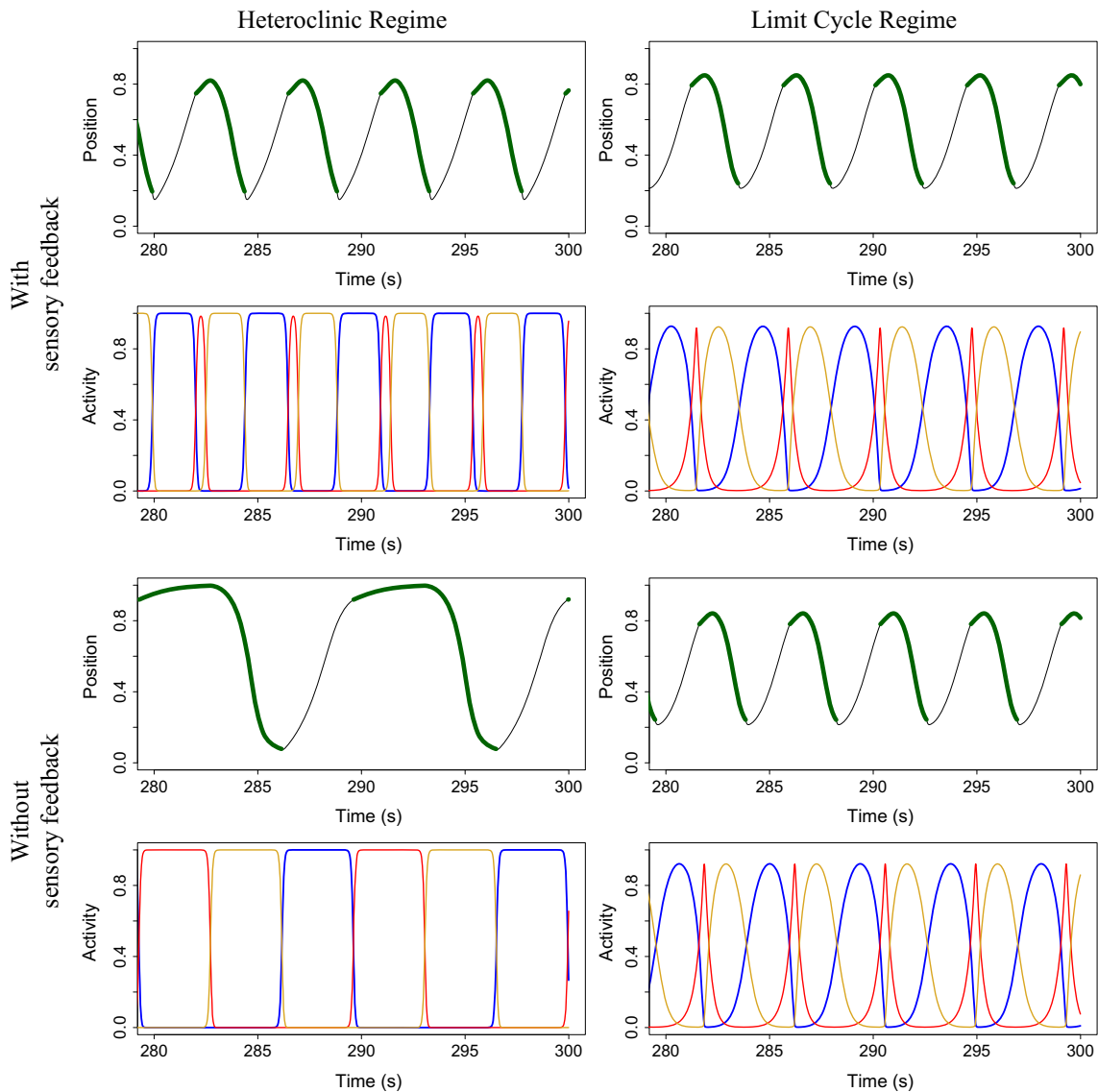


Fig. 14 Removing sensory feedback and endogenous excitation by setting $\epsilon = 0$ and $\mu = 10^{-30}$ slows both protraction and retraction due to the underlying heteroclinic cycle architecture. For reference, the top two panels on the *left and right* show example trajectories for the heteroclinic and limit cycle regimes, respectively (identical to the top panels of Fig. 10). The two panels at *bottom left* show example

trajectories resulting from the removal of sensory input and endogenous excitation ($\epsilon = 0$ and $\mu = 10^{-30}$). When the system is made to resemble a standard limit cycle by setting $\mu = 10^{-3}$, the removal of sensory input no longer has an effect, as seen in the two panels at *bottom right*

slowed cycling in the model (Fig. 14, left), due to the underlying stable heteroclinic channel architecture. In the model, however, when the endogenous excitation of the neurons was increased so that the neural dynamics entered the limit cycle regime, the removal of sensory input had essentially no effect on the model's dynamics (Fig. 14, right). Interestingly, slowed cycling was also observed experimentally in the animal when sensory inputs to the buccal ganglia were removed (Fig. 15). This is consistent with the model in the heteroclinic regime but not the limit cycle regime. Second, the distribution of burst

durations in the model showed a very skewed distribution in the heteroclinic regime but not in the limit cycle regime (Fig. 16). A similarly skewed distribution of retraction durations was observed experimentally *in vivo* (Fig. 17).

6.1 Limitations of the model and results

We have intentionally created a very nominal model of swallowing behavior which does not capture many of the details known about feeding in *Aplysia*. As previous work

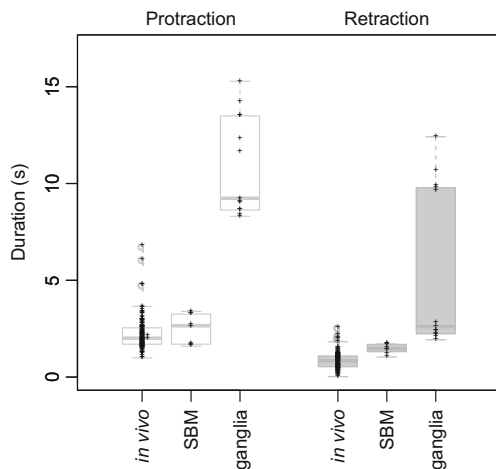


Fig. 15 Protraction and retraction intervals are longer in the suspended buccal mass than in the intact animal, and longer in the isolated ganglia than in either the suspended buccal mass or the intact animal. Bites were used (rather than swallows) because there is no clear analog of a swallow in the isolated ganglia. Medians differ significantly by preparation type for both protraction (Kruskal–Wallis, $p < 0.001$) and retraction (Kruskal–Wallis, $p < 0.001$). Results are similar when swallows from the *in vivo* and suspended buccal mass preparations are used instead of bites (not shown, $p < 0.001$ for both protraction and retraction). Recordings *in vivo*: 146 bites from 6 animals. Suspended buccal mass: 8 bites from 2 animals. Isolated ganglia: 13 motor patterns from 2 animals

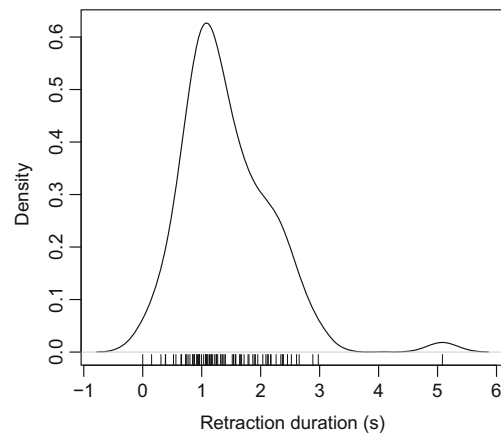


Fig. 17 Retraction durations are significantly skewed during swallowing patterns in intact *Aplysia californica* (skewness = 1.4, D’Agostino test for skewness (D’Agostino et al. 1990): $\sqrt{b_1} = 4.56$, $p < 0.001$). Shown is the kernel density estimator (see the caption to Figure 16 for a description of the algorithm) of the total duration of B6/B9 and B3 activity from 84 swallowing patterns in 6 animals

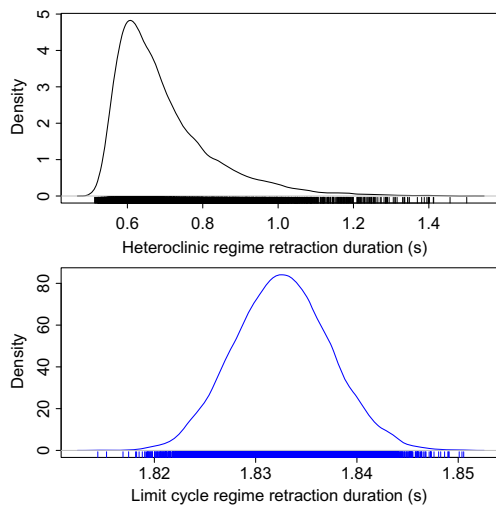


Fig. 16 In the presence of small amounts of noise, retractions are significantly more skewed for the heteroclinic regime than for the limit cycle regime (skewness = 0.91 vs 0.03, for the heteroclinic regime and limit cycle regime respectively). D’Agostino test for skewness (D’Agostino et al. 1990): $\sqrt{b_1} = 32$ vs 1.1, $p < 0.001$ vs $p = 0.27$). Shown is the kernel density estimator for the last a_2 duration in each of 10000 simulations with noise magnitude $\eta = 10^{-4}$. Kernel density estimation was performed using the algorithm given in Silverman (1986), which involves convolving the data with a Gaussian kernel and dividing by the total area of the resulting function. Kernel width was chosen based on the variance of the data (Silverman 1986)

from our lab and others has shown, there are many degrees of biomechanical freedom beyond protraction and retraction that influence the efficacy of feeding (Sutton et al. 2004a, b; Novakovic et al. 2006), the muscles involved have many properties which we do not include in our model (Yu et al. 1999; Zajac 1989), and the mechanics of seaweed are much more complex than we have represented in the model (Denny and Gaylord 2002; Harder et al. 2006). Similarly, the dynamics of proprioception are much more complex than the linear model we have used (Evans and Cropper 1998), and there are more than three pools of neurons involved in feeding behavior (Hurwitz et al. 1997), with dynamics that are much more complex than the firing rate model we have used (Susswein et al. 2002). In addition, neuromodulation and learning may alter the dynamics of the network slowly over time (Nargeot and Simmers 2012; Susswein and Chiel 2012). Thus we expect at best a qualitative match to the *in vivo* behavior, and cannot compare the results against other models as rigorously as could be done with a model capable of quantitative predictions.

A nominal model may also have advantages. As complexity is added to a model, it can become more difficult to interpret the mechanics and, as a result, less clear what details of the dynamics are responsible for an observed aspect of the behavior. In addition, as the parameter space grows, it becomes less obvious how dependent the results are on the particular choice of parameters (Foster et al. 1993). Thus the nominal model we have used makes it clear that passage near a saddle point results in enhanced sensitivity to sensory perturbations, and the role of the parameters in creating these dynamics can be easily understood in an intuitive manner. In addition, the dynamics we have included

in the model, (e.g. mutually inhibitory neural pools, slow antagonistic muscles, and a slow muscle transfer function) are common to many other systems. Thus the qualitative behavior of the model can be more readily generalized to a variety of other systems, which would be more difficult with a highly detailed model.

It is possible that some omitted details are critical for representing the behavior of the actual system. For example, intense bursting in the neural pools involves oscillations in fast variables such as membrane potential and some gating variables. In our model these bursts are represented in terms of passage near a saddle, where the state variables are changing slowly. Many neuronal systems, however, can be decomposed into fast and slow subsystems (Butera et al. 1996; Krupa et al. 2008; Sherwood and Guckenheimer 2010), and slow passages near saddles may occur in the dynamics of the slow state variables, as described by Nowotny and Rabinovich (2007). Ideally, one would want to create a more detailed model of feeding in *Aplysia* and then use a principled reduction to find the slower dynamics. The work done in this paper may be useful for guiding such a reduction.

One should also note that certain features of the experimental data that are well fit by our model based on a stable heteroclinic channel architecture may also be compatible with other dynamical architectures. For example, the skewed distribution of burst durations seen in the heteroclinic regime (Fig. 16) could also be produced by a system in which transitions between a series of stable equilibria are induced by noise. Indeed, attractor networks have been used as models for motor pattern generation (Cruse et al. 1998), and it may be possible to model *Aplysia* feeding using such a system. Further work would need to be done to characterize the respective roles of proprioceptive feedback and endogenous excitation in such systems and to compare them with experimental data. However, the goal of the present work is not to rule out all other possible dynamical architectures consistent with experimental observations. Rather, our emphasis is on proposing the heteroclinic channel architecture as an empirically motivated alternative to the traditional limit cycle formulation of central pattern generators.

6.2 Larger implications for pattern generators

6.2.1 Biological aspects

Many previous authors have noted the difference between patterns seen *in vitro* and those seen *in vivo*, but the field has not yet reached a consensus about the source of these differences. In this paper, we propose that passage of trajectories near a fixed point provides a model that can explain some of the distortions in timing seen *in vitro*. Furthermore,

this dynamical structure may help a pattern generator better use sensory input to adapt to a changing environment, and thus this structure may be selected for by evolutionary pressures. Although stable heteroclinic cycles are not structurally stable and thus are unlikely to be seen in a biological context, stable heteroclinic channels *are* structurally stable and robust to parameter variations and noise (Afraimovich et al. 2004b), and thus they are plausible dynamics for a biological system. The passage near fixed points as a way of controlling timing has been seen in other models, for example (Sparidy et al. 2011c).

Many other pattern generators that have been previously identified may lie between the two extremes on this continuum between ideal central pattern generators and chain reflexes. Slower patterns in the absence of innervation have been seen in lamprey swimming (Wallèn and Williams 1984), crayfish walking (Chrachri and Clarac 1990), and locust flight (Pearson et al. 1983).

These models of pattern generation may also be relevant in clinical contexts. In mammals, fictive respiration can be observed in the isolated central nervous system and is hypothesized to arise from the interaction of two pattern generators in the medulla – an inspiratory pattern generator in the pre-Bötzinger complex and an expiratory pattern generator in the retrotrapezoidal-parafacial area (Tomori et al. 2010). It has been known for some time, however, that vagotomy (cutting the vagus nerve, which contains sensory afferents involved in respiration) causes a dramatic slowing, but not cessation, of respiration. Qualitatively, this behavior is much closer to what we have shown in the stable heteroclinic channel model, and not that of an idealized limit cycle. This would suggest that small perturbations may be enough to cause the changes seen in central sleep apnea and possibly sudden infant death syndrome, but also suggests that the system may remain quite sensitive to certain perturbations even in the pathological state. In the case of central sleep apnea, good models of the dynamics and sensitivity to sensory input might allow for new treatment modalities such as transcranial direct current stimulation during episodes of apnea or hypopnea.

6.2.2 Mathematical implications

Many of the behaviors we have observed in the stable heteroclinic channel regime may depend primarily on localized regions of the dynamics where the intrinsic dynamics, $f(\mathbf{a}, \mu)$, are smaller than the proprioceptive feedback, $\epsilon g(\mathbf{a}, \mathbf{x})$. When the intrinsic excitability μ is sufficiently strong that $f(\mathbf{a}, \mu) > |\epsilon g(\mathbf{a}, \mathbf{x})|$ for all values of \mathbf{a} and \mathbf{x} , the sensory input will have little effect on the temporal dynamics of the neural system. In this second regime, the neural dynamics are largely insensitive to changes in mechanical load or perturbations.

Although we have used a stable heteroclinic channel in our model to create localized regions of slowing, several related dynamical architectures may produce similar effects. For example, in a saddle-node bifurcation on an invariant cycle, the flow around a limit cycle slows near a point as one approaches the bifurcation. This slowing may create qualitatively similar behavior.⁵ Other examples may include relaxation oscillators where some parts of the trajectory are much slower than others, e.g. a Van der Pol oscillator (van der Pol 1926), which can create similar regions of sensitivity (Bässler 1986) that may be relevant for motor pattern generation (Rowat and Selverston 1993; Nadim et al. 2011). Half-center oscillator systems can also exhibit localized slowing, which can affect the response of pattern generators to sensory input (Zhang and Lewis 2013; Daun et al. 2009; Daun-Gruhn 2011; Skinner et al. 1994).

Localized regions of slowing may not always be apparent in a model as it is written. For example, many dynamical models, such as bursting cells, may not have localized regions of slowing in the form that they are written, but can be decomposed using fast-slow analysis into state variables that change on different time scales. In these systems, saddle points may exist in the slower state variables that were not apparent in the complete system.

The Equilibrium Point Hypothesis (EPH) states that motor trajectories could be understood as the result of a control process that sets up one or a sequence of biomechanical equilibrium points (Feldman 1966). Typically, the control is set by an unspecified central mechanism that may take into account high-level sensory (visual, auditory) or goal-related information. Our framework is consistent with the EPH. When the system (1–2) has ϵ set to zero, the autonomous central dynamics has a fixed point \mathbf{a}_{tg} for which the target configuration, \mathbf{x}_{tg} , is a fixed point of the biomechanics, i.e. $h(\mathbf{a}_{\text{tg}}, \mathbf{x}_{\text{tg}}) = 0$, with a suitable adjustment in the case of a nonzero load. The incorporation of sensory feedback from the motor apparatus in the EPH is implicit in the setting of the neural equilibrium point.

Recent investigations have explored both experimental and theoretical approaches to understanding how oscillatory pattern generators incorporate sensory feedback. Daun-Gruhn and Büschges emphasize these issues in modeling approaches to understanding control of stepping motions in insects. As they point out, successful walking on irregular

terrain requires coordinated activation of multiple muscle groups within each limb, as well as coordination between limbs. In the stick insect system, it has been shown that sensory feedback carries information both about joint position and about external loads, and that this feedback impacts both the timing and intensity of motor neuron activation (Büschges and Gruhn 2007; Daun-Gruhn and Büschges 2011). Furthermore, Daun-Gruhn and colleagues discuss how changing a single parameter representing endogenous excitation can cause a half-center oscillator system to transition from a stable limit cycle regime to a regime in which initiation of each phase of the oscillation is contingent on a transient sensory input signal, analogous to a discontinuous bistable chain reflex model (Daun et al. 2009; Daun-Gruhn 2011). In addition, Paoletti and Mahadevan have recently proposed a model for the coordination of peristaltic contractions underlying crawling motility in soft bodied organisms. In their model, coordination of central neural activation between adjacent body segments is mediated not by synaptic connections, but by mechanical interactions affecting the neural elements via sensory feedback through stretch receptors (Paoletti and Mahadevan 2014).

Understanding how sensitivity to perturbations differs in the heteroclinic and limit cycle regimes may also prove useful as a diagnostic tool for probing the intrinsic dynamics of the pattern generating circuit. It has been shown in other cases that phase response curves can provide useful insights into the underlying dynamics of oscillatory pattern generators. For example, Zhang and Lewis (2013) have shown that the phase response curves of half-center oscillator (HCO) circuits can be used to determine whether progression through the cycle is governed by an “escape” or a “release” type mechanism (Wang and Rinzel 1992). They found that in the escape-dominated regime, the system was sensitive to perturbations to the inactive cell as it was becoming active, whereas in the release-dominated regime the opposite was true. Furthermore, they demonstrated that the sensitivity of their system to external inputs resulted from the presence of fixed points near the limit cycle in phase space, which is analogous to what we have observed in our heteroclinic channel model. It remains to be seen whether the oscillations in our model are governed primarily by release or escape and how this depends upon the balance of endogenous excitation and proprioceptive feedback. It may also be useful to compare the phase response curves of the uncoupled neural system to those obtained when proprioceptive feedback is present. As we have shown elsewhere, one can analyze the infinitesimal phase response curve for an uncoupled heteroclinic channel model (Shaw et al. 2012).

⁵The similarity actually goes deeper than this; if one adds a new state variable representing the bifurcation parameter μ and sets $d\mu/dt = 0$, the limit cycle in the augmented system now passes near a degenerate saddle at $\mu = 0$.

Acknowledgments This work was partially supported by the National Science Foundation (grants DMS-1010434 and IIS-1065489), the National Institute of Neurological Disorders and Stroke

(grant NS047073), the Simons Foundation (grant 259837 to Peter Thomas), by the Council for the International Exchange of Scholars (CIES), and by sabbatical support from Case Western Reserve University. Jeffrey Gill was supported by the Graduate Assistance in Areas of National Need program (P200A090191-11), Kendrick Shaw was partially supported by NIH grant T32-GM00725 and David Lyttle was supported by an NSF Postdoctoral Fellowship (grant 1309380).

We are also grateful for helpful discussions with A. Horchler, A. Büschges and S. Daun-Gruhn, and for the comments of two anonymous reviewers on an earlier version of the manuscript.

Conflict of interests The authors declare that they have no conflict of interest.

Appendix A Mathematical framework

Here we present the full model equations for the reader’s convenience, and spell out how our model fits within the general framework presented in Section 2. In this framework, the coupled neuromechanical system is written in the form:

$$\frac{d\mathbf{a}}{dt} = f(\mathbf{a}, \mu) + \epsilon g(\mathbf{a}, \mathbf{x}), \tag{27}$$

$$\frac{d\mathbf{x}}{dt} = h(\mathbf{a}, \mathbf{x}) + \zeta l(\mathbf{x}). \tag{28}$$

In the specific example studied here, the vector \mathbf{a} of neural variables consists of $a_0, a_1,$ and a_2 . The full equations for the neural state variables a_i (noiseless case) are:

$$\frac{da_0}{dt} = \frac{1}{\tau_a}(a_0(1 - a_0 - \gamma a_1) + \mu) + \epsilon(x_r - S_0)\sigma_0, \tag{29}$$

$$\frac{da_1}{dt} = \frac{1}{\tau_a}(a_1(1 - a_1 - \gamma a_2) + \mu) + \epsilon(x_r - S_1)\sigma_1, \tag{30}$$

$$\frac{da_2}{dt} = \frac{1}{\tau_a}(a_2(1 - a_2 - \gamma a_0) + \mu) + \epsilon(x_r - S_2)\sigma_2. \tag{31}$$

These equations apply when $a_i \in (0, 1)$. At the boundaries, strict rectifying boundary conditions are imposed which prevent a_i from being greater than 1 or less than 0. Specifically, when a neural variable is at 0, any further inhibitory input has no effect. Similarly, when a variable is at 1, any additional excitatory input has no effect. In the stochastic form of the equations each equation is amended to include a ηdW_i term.

Relating Eqs. (29–31) to Eq. (27) is straightforward. Here

$$f_i(\mathbf{a}, \mu) = \frac{1}{\tau_a}(a_i(1 - a_i - \gamma a_{i+1}) + \mu), \tag{32}$$

and

$$\epsilon g_i(\mathbf{a}, \mathbf{x}) = \epsilon(x_r - S_i)\sigma_i. \tag{33}$$

The vector of mechanical state variables \mathbf{x} consists of u_0, u_1, x_r and a binary variable ψ which takes the value of 0 or

1 depending on whether the grasper is open or closed. The equations for the muscle activation variables u_i are:

$$\frac{du_0}{dt} = \frac{1}{\tau_m}((a_0 + a_1)u_{\max} - u_0), \tag{34}$$

$$\frac{du_1}{dt} = \frac{1}{\tau_m}(a_2u_{\max} - u_1). \tag{35}$$

Note that u_0 activates the I2 muscle (protraction) and u_1 activates the I3 muscle (retraction). The grasper can be either open or closed. When $a_1 + a_2 > 0.5$, it is closed ($\psi = 0$), otherwise it is open ($\psi = 1$).

The position of the grasper (x_r) is governed by the equation

$$\frac{dx_r}{dt} = \frac{F_{\text{musc}}}{b_r} \tag{36}$$

when the grasper is open, and

$$\frac{dx_r}{dt} = \frac{F_{\text{musc}} + F_{\text{sw}}}{b_r + b_{\text{sw}}} \tag{37}$$

when it is closed. This can be written in terms of a single equation as

$$\frac{dx_r}{dt} = \frac{F_{\text{musc}}}{b_r + \psi b_{\text{sw}}} + \psi \frac{F_{\text{sw}}}{b_r + b_{\text{sw}}}. \tag{38}$$

The grasper position is also subject to the rectifying boundary conditions that prevent it from going above 1 or below 0.

The muscle force F_{musc} is the sum of the I2 and I3 muscles, given by

$$F_{\text{musc}} = \sum_i k_i \phi\left(\frac{x_r - c_i}{w_i}\right) u_i \tag{39}$$

where $\phi(x) = -\kappa x(x - 1)(x + 1)$ is the length-tension curve of the muscles (with $\kappa = 3\sqrt{3}/2$), and $i = 0, 1$ denote the I2 and I3 muscles, respectively. Here $x_r \in [0, 1]$ is the position of the grasper, k_i is a parameter representing the strength and direction of each muscle, c_i the position of the grasper where the i th muscle is at its minimum effective length, and w_i the difference between the maximum and minimum effective lengths for the i th muscle. The sign of k_i determines the direction of force of the muscle; when k_i is negative (as it is for I2) the muscle will shorten as it move the grasper forward toward the anterior portion of the jaws (protraction), and when it is positive (as it is for I3) it will shorten as it moves the grasper backward toward the posterior portion of the jaws (retraction).

Relating Eqs. (34–39) to Eq. (28), one can see that $h(\mathbf{a}, \mathbf{x})$ includes the equations governing the u_i variables, the switch determining the open/closed state of the grasper, as well as the equation governing x_r . The term $\zeta l(\mathbf{x})$ refers to the applied load, which is $\psi F_{\text{sw}}/(b_r + b_{\text{sw}})$.

Appendix B Derivation of simplified biomechanics

The seaweed and grasper are assigned viscous damping constants b_{sw} and b_r , respectively; thus the full equations of motion are

$$\frac{dx_r}{dt} = v_r, \tag{40}$$

$$\frac{dx_{sw}}{dt} = 0, \tag{41}$$

$$\frac{dv_r}{dt} = \frac{F_{musc} - b_r v_r}{m_r}, \tag{42}$$

$$\frac{dv_{sw}}{dt} = 0 \tag{43}$$

when the grasper is open, and

$$\frac{dx_r}{dt} = \frac{dx_{sw}}{dt} = v_r, \tag{44}$$

$$\frac{dv_r}{dt} = \frac{F_{musc} + F_{sw} - (b_r + b_{sw})v_r}{m_r + m_{sw}}, \tag{45}$$

$$v_{sw} = v_r \tag{46}$$

when the grasper is closed. Note that that we are assuming that the momentum of the seaweed is negligible and that the seaweed is stationary when the grasper is open.

Table 1 Model parameters

Parameter	Value	Description
γ	2.4	inhibition strength from next pool
ϵ	0.002	sensory feedback strength
κ	$3\sqrt{3}/2$	length-tension curve normalization constant
μ	10^{-9}	neural pool intrinsic excitation
τ_a	0.05	neural pool time constant
τ_m	2.45	muscle activation time constant
b_r	0.1	grasper damping constant
b_{sw}	0.3	seaweed damping constant
c_0	1.0	position of shortest length for I2
c_1	1.1	position of center of I3
F_{sw}	0.01	force on the seaweed resisting ingestion
k_0	-1	I2 muscle strength and direction
k_1	1	I3 muscle strength and direction
σ_0	-1	sign of proprioceptive input to a_0 neural pool
σ_1	1	sign of proprioceptive input to a_1 neural pool
σ_2	1	sign of proprioceptive input to a_2 neural pool
S_0	0.5	proprioceptive neutral position for protraction open neural pool
S_1	0.5	proprioceptive neutral position for protraction closing neural pool
S_2	0.25	proprioceptive neutral position for retraction closed neural pool
u_{max}	1.0	maximum muscle activation
w_0	2	maximal effective length of I2
w_1	1.1	maximal effective length of I3

Table 2 State variables

State variable	Initial value	Description
a_0	$1 - 10^{-9}$	activity of protraction open neural pool (non-negative)
a_1	10^{-9}	activity of protraction closing neural pool (non-negative)
a_2	10^{-9}	activity of retraction closed neural pool (non-negative)
u_0	0	activity of I2 muscle
u_1	0	activity of I3 muscle
x_r	0.5	grasper position (0 is retracted, 1 is protracted)
x_{sw}	0	seaweed position (positive is away from the animal)

Under the assumption that the system is critically damped, we can then use the following reduced system:

$$\frac{dx_r}{dt} = \frac{F_{musc}}{b_r}, \tag{47}$$

$$\frac{dx_{sw}}{dt} = 0 \tag{48}$$

when the grasper is open, and

$$\frac{dx_{sw}}{dt} = \frac{dx_r}{dt} = \frac{F_{musc} + F_{sw}}{b_r + b_{sw}} \tag{49}$$

when the grasper is closed.

Appendix C Parameters and state variables

The meaning and default values of all the parameters (for the heteroclinic regime) are given in the following table:

In the limit cycle regime, the neural time constant is rescaled by replacing the neural time constant τ_a with the following activity-dependent time scaling function:

$$\tau_a(\mathbf{a}) = (1 + \boldsymbol{\alpha} \cdot \mathbf{a})\beta \tag{50}$$

where β is a uniform adjustment in the speed of the trajectories (analogous to the previous constant), and $\boldsymbol{\alpha}$ is a vector parameter representing an activity-dependent scaling of the

Table 3 Parameters used for the limit cycle simulations

Parameter	Value	Description
β	0.2262	neural pool global time constant
μ	10^{-3}	neural pool intrinsic excitation
α_0	0.59	neural pool local time scaling near protraction open
α_1	-0.975	neural pool local time scaling near protraction closing
α_2	0.32	neural pool local time scaling near retraction closed
u_{max}	1.6	maximum muscle activation

speed. μ and u_{\max} are also altered. The values used in the limit cycle regime are given in Table 3.

References

- Afraimovich, V., Young, T., Muezzinoglu, M.K., Rabinovich, M.I. (2011). Nonlinear dynamics of emotion-cognition interaction: When emotion does not destroy cognition? *Bulletin of Mathematical Biology*, 73(2), 266–284. doi:10.1007/s11538-010-9572-x.
- Afraimovich, V.S., Rabinovich, M.I., Varona, P. (2004a). Heteroclinic contours in neural ensembles and the winnerless competition principle. *International Journal of Bifurcation and Chaos*, 14(04), 1195–1208. doi:10.1142/S0218127404009806.
- Afraimovich, V.S., Zhigulin, V.P., Rabinovich, M.I. (2004b). On the origin of reproducible sequential activity in neural circuits. *Chaos: An Interdisciplinary Journal of Nonlinear Science*, 14(4), 1123. doi:10.1063/1.1819625. <http://link.aip.org/link/CHAOEH/v14/i4/p1123/s1&Agg=doi>.
- Armbruster, D., Stone, E., Kirk, V. (2003). Noisy heteroclinic networks. *Chaos: An Interdisciplinary Journal of Nonlinear Science*, 13(1), 71–79.
- Ashwin, P., Karabacak, Ö., Nowotny, T. (2011). Criteria for robustness of heteroclinic cycles in neural microcircuits. *The Journal of Mathematical Neuroscience (JMN)*, 1(1), 1–18.
- Bakhtin, Y. (2011). Noisy heteroclinic networks. *Probability Theory and Related Fields*, 150(1–2), 1–42. doi: 10.1007/s00440-010-0264-0.
- Baxter, D.A., & Byrne, J.H. (2006). Feeding behavior of *Aplysia*: A model system for comparing cellular mechanisms of classical and operant conditioning. *Learn Mem*, 13(6), 669–680. doi:10.1101/lm.339206.
- Bässler, U. (1986). On the definition of central pattern generator and its sensory control. *Biological Cybernetics*, 54(1), 65–69. doi:10.1007/BF00337116.
- Büschges, A., & Gruhn, M. (2007). Mechanosensory feedback in walking: From joint control to locomotor patterns. *Advances in Insect Physiology*, 34, 193–230.
- Butera, R.J., Clark, J.W., Byrne, J.H., Rinzler, J. (1996). Dissection and reduction of a modeled bursting neuron. *Journal of Computational Neuroscience*, 3(3), 199–223. doi:10.1007/BF00161132. <http://www.springerlink.com/content/n2733052qjgj5761/>.
- Cataldo, E., Byrne, J., Baxter, D. (2006). Computational model of a central pattern generator. In *Computational methods in systems biology, lecture notes in computer science* (Vol. 4210, pp. 242–256). Berlin / Heidelberg: Springer. doi: 10.1007/11885191_17.
- Chrachri, A., & Clarac, F. (1990). Fictive locomotion in the fourth thoracic ganglion of the crayfish, *Procambarus clarkii*. *The Journal of Neuroscience*, 10(3), 707–719. <http://www.jneurosci.org/content/10/3/707>.
- Church, P.J., & Lloyd, P.E. (1994). Activity of multiple identified motor neurons recorded intracellularly during evoked feeding-like motor programs in *Aplysia*. *Journal of Neurophysiology*, 72(4), 1794–1809. <http://jn.physiology.org/cgi/content/abstract/72/4/1794>.
- Cruse, H., Kindermann, T., Schumm, M., Dean, J., Schmitz, J. (1998). Walknet—a biologically inspired network to control six-legged walking. *Neural Networks*, 11(7), 1435–1447.
- Cullins, M.J., & Chiel, H.J. (2010). Electrode fabrication and implantation in *Aplysia californica* for multi-channel neural and muscular recordings in intact, freely behaving animals. *Journal of Visualized Experiments*, (40), doi:10.3791/1791.
- D’Agostino, R.B., Belanger, A., D’Agostino, R.B. (1990). A suggestion for using powerful and informative tests of normality. *The American Statistician*, 44(4), 316–321. doi:10.2307/2684359.
- Daun, S., Rubin, J.E., Rybak, I.A. (2009). Control of oscillation periods and phase durations in half-center central pattern generators: A comparative mechanistic analysis. *Journal of Computational Neuroscience*, 27(1), 3–36.
- Daun-Gruhn, S. (2011). A mathematical modeling study of intersegmental coordination during stick insect walking. *Journal of Computational Neuroscience*, 30(2), 255–278.
- Daun-Gruhn, S., & Büschges, A. (2011). From neuron to behavior: Dynamic equation-based prediction of biological processes in motor control. *Biological Cybernetics*, 105(1), 71–88.
- Denny, M., & Gaylord, B. (2002). The mechanics of wave-swept algae. *Journal of Experimental Biology*, 205(10), 1355–1362. <http://jeb.biologists.org/content/205/10/1355>.
- Di Bernardo, M., Budd, C.J., Champneys, A.R., Kowalczyk, P., Nordmark, A.B., Tost, G.O., Piironen, P.T. (2008). Bifurcations in nonsmooth dynamical systems. *Siam Review*, 629–701.
- Evans, C.G., & Cropper, E.C. (1998). Proprioceptive input to feeding motor programs in *Aplysia*. *Journal of Neuroscience*, 18(19), 8016–8031. <http://www.jneurosci.org/cgi/content/abstract/18/19/8016>.
- Feldman, A.G. (1966). Functional tuning of the nervous system with control of movement or maintenance of a steady posture. II. Controllable parameters of the muscle. *Biophysics*, 11(3), 565–578.
- Forssberg, H. (1979). Stumbling corrective reaction: A phase-dependent compensatory reaction during locomotion. *Journal of Neurophysiology*, 42(4), 936–953. <http://jn.physiology.org/content/42/4/936>.
- Forssberg, H., Grillner, S., Rossignol, S. (1975). Phase dependent reflex reversal during walking in chronic spinal cats. *Brain Research*, 85(1), 103–107. http://journals.ohiolink.edu/ejc/article.cgi?issn=00068993&issue=v85i0001&article=103_pdrdrwicsc.
- Foster, W.R., Ungar, L.H., Schwaber, J.S. (1993). Significance of conductances in Hodgkin-Huxley models. *Journal of Neurophysiology*, 70(6), 2502–2518. <http://jn.physiology.org/content/70/6/2502>.
- Fox, L.E., & Lloyd, P.E. (1997). Serotonin and the small cardioactive peptides differentially modulate two motor neurons that innervate the same muscle fibers in *Aplysia*. *The Journal of Neuroscience*, 17(16), 6064–6074. <http://www.jneurosci.org/content/17/16/6064>.
- Gog, J., Oprea, I., Proctor, M., Rucklidge, A. (1999). Destabilization by noise of transverse perturbations to heteroclinic cycles: A simple model and an example from dynamo theory. *Proceedings of the Royal Society of London Series A: Mathematical, Physical and Engineering Sciences*, 455(1992), 4205–4222.
- Goldwyn, J.H., & Shea-Brown, E. (2011). The what and where of adding channel noise to the Hodgkin-Huxley equations. *PLoS Computational Biology*, 7(11), e1002247. doi: 10.1371/journal.pcbi.1002247.
- Gordon, A.M., Huxley, A.F., Julian, F.J. (1966). The variation in isometric tension with sarcomere length in vertebrate muscle fibres. *The Journal of Physiology*, 184(1), 170–192. <http://jp.physoc.org/content/184/1/170>.
- Guckenheimer, J., & Holmes, P. (1988). Structurally stable heteroclinic cycles. *Mathematical Proceedings of the Cambridge Philosophical Society*, 103(01), 189–192. doi: 10.1017/S0305004100064732.

- Harder, D.L., Hurd, C.L., Speck, T. (2006). Comparison of mechanical properties of four large, wave-exposed seaweeds. *American Journal of Botany*, 93(10), 1426–1432. doi:10.3732/ajb.93.10.1426.
- Harri, M., & Florey, E. (1977). The effects of temperature on a neuromuscular system of the crayfish, *Astacus leptodactylus*. *Journal of Comparative Physiology*, 117(1), 47–61. doi:10.1007/BF00605523.
- Hurwitz, I., Neustadter, D., Morton, D.W., Chiel, H.J., Susswein, A.J. (1996). Activity patterns of the B31/B32 pattern initiators innervating the I2 muscle of the buccal mass during normal feeding movements in *Aplysia californica*. *Journal of Neurophysiology*, 75(4), 1309–26.
- Hurwitz, I., Kupfermann, I., Susswein, A.J. (1997). Different roles of neurons B63 and B34 that are active during the protraction phase of buccal motor programs in *Aplysia californica*. *Journal of Neurophysiology*, 78(3), 1305–1319. <http://jn.physiology.org/content/78/3/1305.abstract>.
- Ijspeert, A.J. (2008). Central pattern generators for locomotion control in animals and robots: A review. *Neural Networks*, 21(4), 642–653. doi:10.1016/j.neunet.2008.03.014.
- Jing, J., Cropper, E.C., Hurwitz, I., Weiss, K.R. (2004). The construction of movement with behavior-specific and behavior-independent modules. *The Journal of neuroscience*, 24(28), 6315–6325.
- Kloeden, P.E., & Platen, E. (1992). *Numerical solution of stochastic differential equations*. Berlin: Springer-Verlag.
- Komarov, M., Osipov, G., Suykens, J. (2009). Sequentially activated groups in neural networks. *EPL (Europhysics Letters)*, 86(6), 60,006.
- Komarov, M., Osipov, G., Suykens, J. (2010). Metastable states and transient activity in ensembles of excitatory and inhibitory elements. *EPL (Europhysics Letters)*, 91(2), 20,006.
- Komarov, M., Osipov, G., Zhou, C. (2013). Heteroclinic contours in oscillatory ensembles. *Physical Review E*, 87(2), 022,909.
- Kori, H., & Kuramoto, Y. (2001). Slow switching in globally coupled oscillators: Robustness and occurrence through delayed coupling. *Physical Review E*, 63(4), 046,214.
- Krupa, M., Popović, N., Kopell, N., Rotstein, H.G. (2008). Mixed-mode oscillations in a three time-scale model for the dopaminergic neuron. *Chaos: An Interdisciplinary Journal of Nonlinear Science*, 18(1), 015,106–015,106–19. doi:10.1063/1.2779859. http://chaos.aip.org/resource/1/chaoh/v18/i1/p015106_s1.
- Levi, R., Varona, P., Arshavsky, Y.I., Rabinovich, M.I., Selverston, A.I. (2004). Dual sensory-motor function for a molluscan statocyst network. *Journal of Neurophysiology*, 91(1), 336–345. doi:10.1152/jn.00753.2003. <http://jn.physiology.org/cgi/content/abstract/91/1/336>.
- Lewinger, W.A., Rutter, B.L., Blümel, M., Büschges, A., Quinn, R.D. (2006). Sensory coupled action switching modules (SCASM) generate robust, adaptive stepping in legged robots. In: *Proceedings of the 9th international conference on climbing and walking robots (CLAWAR'06)* (pp. 661–71). Brussels.
- Loeb, J. (1899). Einleitung in die vergleichende Gehirnphysiologie und vergleichende psychologie, mit besonderer berücksichtigung der wirbellosen thiere. Leipzig, J.A. Barth, <http://archive.org/details/einleitungindiev00loeb>.
- Lu, H., McManus, J.M., Chiel, H.J. (2013). Extracellularly identifying motor neurons for a muscle motor pool in *Aplysia californica*. *Journal of Visualized Experiments*, (73), doi:10.3791/50189.
- Makarenkov, O., & Lamb, J.S. (2012). Dynamics and bifurcations of nonsmooth systems: A survey. *Physica D: Nonlinear Phenomena*, 241(22), 1826–1844.
- Marder, E., & Bucher, D. (2001). Central pattern generators and the control of rhythmic movements. *Current Biology*, 11(23), R986–R996. doi:10.1016/S0960-9822(01)00581-4.
- Matsumoto, M., & Nishimura, T. (1998). Mersenne twister: A 623-dimensionally equidistributed uniform pseudo-random number generator. *ACM Transactions Model Computation and Simulation*, 8(1), 3–30. doi:10.1145/272991.272995.
- McManus, J.M., Lu, H., Chiel, H.J. (2012). An *in vitro* preparation for eliciting and recording feeding motor programs with physiological movements in *Aplysia californica*. *Journal of Visualized Experiments*, (70), doi:10.3791/4320.
- McManus, J.M., Lu, H., Cullins, M.J., Chiel, H.J. (2014). Differential activation of an identified motor neuron and neuromodulation provide *Aplysia's* retractor muscle an additional function. *Journal of Neurophysiology*. In press.
- Morton, D.W., & Chiel, H.J. (1993). The timing of activity in motor neurons that produce radula movements distinguishes ingestion from rejection in *Aplysia*. *Journal of Comparative Physiology A: Neuroethology, Sensory Neural, and Behavioral Physiology*, 173(5), 519–536. doi:10.1007/BF00197761.
- Nadim, F., Zhao, S., Zhou, L., Bose, A. (2011). Inhibitory feedback promotes stability in an oscillatory network. *Journal of neural engineering*, 8(6), 065,001.
- Nargeot, R., & Simmers, J. (2012). Functional organization and adaptability of a decision-making network in *Aplysia*. *Frontiers in Neuroscience*, 6. doi:10.3389/fnins.2012.00113. <http://www.ncbi.nlm.nih.gov/pmc/articles/PMC3405415/>.
- Neustadter, D.M., Drushel, R.F., Chiel, H.J. (2002). Kinematics of the buccal mass during swallowing based on magnetic resonance imaging in intact, behaving *Aplysia californica*. *Journal of Experimental Biology*, 205(7), 939–958. <http://jeb.biologists.org/cgi/content/abstract/205/7/939>.
- Neustadter, D.M., Herman, R.L., Drushel, R.F., Chestek, D.W., Chiel, H.J. (2007). The kinematics of multifunctionality: Comparisons of biting and swallowing in *Aplysia californica*. *Journal of Experimental Biology*, 210(2), 238–260. doi:10.1242/jeb.02654. <http://jeb.biologists.org/cgi/content/abstract/210/2/238>.
- Novak, B., Csikasz-Nagy, A., Györfy, B., Nasmyth, K., Tyson, J.J. (1998). Model scenarios for evolution of the eukaryotic cell cycle. *Philosophical Transactions of the Royal Society of London Series B: Biological Sciences*, 353(1378), 2063–2076. doi:10.1098/rstb.1998.0352. <http://rstb.royalsocietypublishing.org/content/353/1378/2063>.
- Novakovic, V.A., Sutton, G.P., Neustadter, D.M., Beer, R.D., Chiel, H.J. (2006). Mechanical reconfiguration mediates swallowing and rejection in *Aplysia californica*. *Journal of Comparative Physiology A: Neuroethology, Sensory Neural, and Behavioral Physiology*, 192(8), 857–870. doi:10.1007/s00359-006-0124-7.
- Nowotny, T., & Rabinovich, M.I. (2007). Dynamical origin of independent spiking and bursting activity in neural microcircuits. *Physical Review Letters*, 98(12), 128,106–4. doi:10.1103/PhysRevLett.98.128106. <http://link.aps.org/abstract/PRL/v98/e128106>.
- Paoletti, P., & Mahadevan, L. (2014). A proprioceptive neuromechanical theory of crawling. *Journal of the Royal Society Interface*. In press.
- Pearson, K.G., Reye, D.N., Robertson, R.M. (1983). Phase-dependent influences of wing stretch receptors on flight rhythm in the locust. *Journal of Neurophysiology*, 49(5), 1168–1181. <http://post.queensu.ca/locust/Publications/pearson%20reye%20robertson%201983%20jnp.pdf>.
- van der Pol, B. (1926). On “relaxation-oscillations”. *Philosophical Magazine Series 7*, 2(11), 978–992. doi: 10.1080/14786442608564127.

- Rabinovich, M.I., Huerta, R., Varona, P., Afraimovich, V.S. (2008). Transient cognitive dynamics, metastability, and decision making. *PLoS Computational Biology*, 4(5), e1000072. doi: [10.1371/journal.pcbi.1000072](https://doi.org/10.1371/journal.pcbi.1000072).
- Reyn, J.W. (1980). Generation of limit cycles from separatrix polygons in the phase plane. In: R. Martini (Ed.), *Geometrical approaches to differential equations, no. 810 in lecture notes in mathematics*, (pp. 264–289). Berlin Heidelberg: Springer. <http://link.springer.com/chapter/10.1007/BFb0089983>.
- Rawat, P.F., & Selverston, A. (1993). Modeling the gastric mill central pattern generator of the lobster with a relaxation-oscillator network. *Journal of Neurophysiology*, 70(3).
- Sacco, P., McIntyre, D.B., Jones, D.A. (1994). Effects of length and stimulation frequency on fatigue of the human tibialis anterior muscle. *Journal of Applied Physiology*, 77(3), 1148–1154. <http://jap.physiology.org/content/77/3/1148>.
- Schiff, S.J. (2012). *Neural control engineering: The emerging intersection between control theory and neuroscience*. Cambridge: MIT Press. <http://search.ebscohost.com/login.aspx?direct=true&scope=site&db=nlebk&db=nlabk&AN=512645>.
- Selverston, A.I. (1985). *Model neural networks and behavior*. New York: Plenum Press.
- Shaw, K.M., Park, Y.M., Chiel, H.J., Thomas, P.J. (2012). Phase resetting in an asymptotically phaseless system: On the phase response of limit cycles verging on a heteroclinic orbit. *SIAM Journal on Applied Dynamical Systems*, 11, 350–391. doi: [10.1137/110828976](https://doi.org/10.1137/110828976). <http://link.aip.org/link/?SJA/11/350/1>.
- Sherrington, C.S. (1910). Flexion-reflex of the limb, crossed extension-reflex, and reflex stepping and standing. *The Journal of Physiology*, 40(1–2), 28–121. <http://www.ncbi.nlm.nih.gov/pmc/articles/PMC1533734/>.
- Sherwood, W.E., & Guckenheimer, J. (2010). Dissecting the phase response of a model bursting neuron. *SIAM Journal on Applied Dynamical Systems*, 9(3), 659–703. <http://epubs.siam.org/doi/abs/10.1137/090773519>.
- Shilnikov, L.P., Shilnikov, A.L., Turaev DV, Chua LO (2002). Methods of qualitative theory in nonlinear dynamics, Part II. World Scientific.
- Silverman, B.W. (1986). *Density estimation for statistics and data analysis* (Vol. 26). CRC Press.
- Skinner, F.K., Kopell, N., Marder, E. (1994). Mechanisms for oscillation and frequency control in reciprocally inhibitory model neural networks. *Journal of Computational Neuroscience*, 1(1–2), 69–87.
- Sparidy, L.E., Markin, S.N., Shevtsova, N.A., Prilutsky, B.I., Rybak, I.A., Rubin, J.E. (2011a). A dynamical systems analysis of afferent control in a neuromechanical model of locomotion. I. Rhythm generation. *Journal of Neural Engineering*, 8(6), 065,003.
- Sparidy, L.E., Markin, S.N., Shevtsova, N.A., Prilutsky, B.I., Rybak, I.A., Rubin, J.E. (2011b). A dynamical systems analysis of afferent control in a neuromechanical model of locomotion. II. Phase asymmetry. *Journal of Neural Engineering*, 8(6), 065,004.
- Sparidy, L.E., Markin, S.N., Shevtsova, N.A., Prilutsky, B.I., Rybak, I.A., Rubin, J.E. (2011c). A dynamical systems analysis of afferent control in a neuromechanical model of locomotion: II. phase asymmetry. *Journal of Neural Engineering*, 8(6), 065,004. doi: [10.1088/1741-2560/8/6/065004](https://doi.org/10.1088/1741-2560/8/6/065004).
- Stone, E., & Holmes, P. (1990). Random perturbations of heteroclinic attractors. *SIAM Journal on Applied Mathematics*, 50(3), 726–743. doi: [10.2307/2101884](https://doi.org/10.2307/2101884). <http://www.jstor.org/stable/2101884>.
- Susswein, A.J., & Chiel, H.J. (2012). Nitric oxide as a regulator of behavior: New ideas from *Aplysia* feeding. *Progress in Neurobiology*, 97(3), 304–317. doi: [10.1016/j.pneurobio.2012.03.004](https://doi.org/10.1016/j.pneurobio.2012.03.004). <http://www.sciencedirect.com/science/article/pii/S0301008212000366>.
- Susswein, A.J., Hurwitz, I., Thorne, R., Byrne, J.H., Baxter, D.A. (2002). Mechanisms underlying fictive feeding in *Aplysia*: Coupling between a large neuron with plateau potentials activity and a spiking neuron. *Journal of Neurophysiology*, 87(5), 2307–2323. <http://jn.physiology.org/content/87/5/2307.long>.
- Sutton, G.P., Macknin, J.B., Gartman, S.S., Sunny, G.P., Beer, R.D., Crago, P.E., Neustadter, D.M., Chiel, H.J. (2004a). Passive hinge forces in the feeding apparatus of *Aplysia* aid retraction during biting but not during swallowing. *Journal of Comparative Physiology A*, 190(6), 501–514. doi: [10.1007/s00359-004-0517-4](https://doi.org/10.1007/s00359-004-0517-4).
- Sutton, G.P., Mangan, E.V., Neustadter, D.M., Beer, R.D., Crago, P.E., Chiel, H.J. (2004b). Neural control exploits changing mechanical advantage and context dependence to generate different feeding responses in *Aplysia*. *Biological Cybernetics*, 91(5), 333–345. doi: [10.1007/s00422-004-0517-z](https://doi.org/10.1007/s00422-004-0517-z).
- Tomori, Z., Poliacek, I., Jakus, J., Widdicombe, J., Donic, V., Benacka, R., Gresova, S. (2010). Distinct generators for aspiration and expiration reflexes: Localization, mechanisms and effects. *Journal of Physiology and Pharmacology: An Official Journal of the Polish Physiological Society*, 61(1), 5–12.
- Vandorpe, D.H., Small, D.L., Dabrowski, A.R., Morris, C.E. (1994). FMRFamide and membrane stretch as activators of the *Aplysia* S-channel. *Biophysical Journal*, 66(1), 46–58. <http://www.ncbi.nlm.nih.gov/pmc/articles/PMC1275662/>.
- Varona, P., Levi, R., Arshavsky, Y.I., Rabinovich, M.I., Selverston, A.I. (2004). Competing sensory neurons and motor rhythm coordination. *Neurocomputing*, 58–60, 549–554. doi: [10.1016/j.neucom.2004.01.093](https://doi.org/10.1016/j.neucom.2004.01.093). <http://www.sciencedirect.com/science/article/B6V10-4BVP69M-M/2/c7aa0434cb0551bbe9ac6b1707b52ba7>.
- Wallèn, P., & Williams, T.L. (1984). Fictive locomotion in the lamprey spinal cord *in vitro* compared with swimming in the intact and spinal animal. *The Journal of Physiology*, 347(1), 225–239. <http://jp.physoc.org/content/347/1/225>.
- Wang, X.J., & Rinzler, J. (1992). Alternating and synchronous rhythms in reciprocally inhibitory model neurons. *Neural Computation*, 4(1), 84–97.
- White, J., Rubinstein, J., Kay, A. (2000). Channel noise in neurons. *Trends Neuroscience*, 23, 131–137.
- Williams, C.D., Salcedo, M.K., Irving, T.C., Regnier, M., Daniel, T.L. (2013). The length–tension curve in muscle depends on lattice spacing. *Proceedings of the Royal Society B: Biological Sciences*, 280(1766). doi: [10.1098/rspb.2013.0697](https://doi.org/10.1098/rspb.2013.0697).
- Wilson, D.M. (1961). The central nervous control of flight in a locust. *Journal of Experimental Biology*, 38(2), 471–490. <http://jeb.biologists.org/content/38/2/471>.
- Yu, S.N., Crago, P.E., Chiel, H.J. (1999). Biomechanical properties and a kinetic simulation model of the smooth muscle I2 in the buccal mass of *Aplysia*. *Biological Cybernetics*, 81(5–6), 505–513.
- Zajac, F.E. (1989). Muscle and tendon: properties, models, scaling, and application to biomechanics and motor control. *Critical Reviews in Biomedical Engineering*, 17(4), 359–411.
- Zhang, C., & Lewis, T.J. (2013). Phase response properties of half-center oscillators. *Journal of Computational Neuroscience*, 35(1), 55–74.